DURBAN UNIVERSITY OF TECHNOLOGY

OPTIMISATION OF HYBRID MICRO-GRID SYSTEM FOR LTE BASE STATION

By

Sempe Thom Leholo

Student Number: 21855573

A dissertation submitted in the fulfilment of the requirements for the degree of Master of Engineering in Electrical Power Engineering

In the Department of Electrical Power Engineering

Faculty of Engineering and the Built Environment

Supervisor: Prof. P.A. Owolawi

Co-Supervisor: Mr. K.T. Akindeji

2020

DECLARATION

I hereby declare that this dissertation is my work, and each text has been correctly referenced or cited. Moreover, this work has not been previously published in portion or whole for another degree at any other University.

This research was duly supervised by Professor P.A. Owolawi and Mr K.T. Akindeji at the Durban University of Technology.

Submitted by:

……. ……..……..

S. T. Leholo Date

Student Number: 21855573

Approved for Final Submission by:

……. …….

Supervisor: Prof. P. A. Owolawi Date

……. …….

Co-Supervisor: Mr. K.T Akindeji Date

DEDICATION

This work is dedicated to:

My supportive and loving wife;

The blessed memory of my late mother and ever-supportive siblings;

My colleagues; and

My friends.

ACKNOWLEDGEMENTS

I want to start by giving the Almighty God the praise for giving me the strength and wisdom to complete my postgraduate programme.

I would like to start by thanking my supervisor, Professor Pius Adewale Owolawi, and my co-supervisor Mr Timothy Kayode Akindeji, for their generous support, patience, motivation, guidance and uplifting assistance during the entire journey of my study. I would also love to convey my most genuine gratitude to the Durban University of Technology for providing me with all the necessary resources to make my postgraduate programme a success.

I would furthermore like to thank my colleagues for their continuous support as well as for helping me to make my academic life pleasurable throughout my studies. A special thanks to my colleagues at the Tshwane University of Technology who have generously assisted me to accomplish my academic achievement by providing me with administrative, morale, motivation and resources support.

In addition, I would like to take this opportunity to thank my wife, Lebogang Leholo and the rest of my family for their support as well as motivation throughout this study. I am indebted to those people who directly or indirectly contributed to the success of this programme.

Finally, I acknowledge the financial support for this work provided by the Tshwane University of Technology and Durban University of Technology. I thank you all.

ABSTRACT

This study explores the prospect of powering a Long-Term Evolution (LTE) base transceiver station (LTE BTS) with a Hybrid Renewable Energy System (HRES) in the rural areas of South Africa. The focus of the study is on harnessing the inherent advantage in HRES which in return reduces the Greenhouse Gas (GHG) emissions and operational costs associated with a Diesel Generator (DG) used to power LTE BTS in the rural areas. Moreover, the HRES will help with enhancing stability, reliability, and sustainability of electric power supply to fulfil the required LTE BTS loads. Hence, the proposed HRES consists of Photovoltaic (PV) system, Wind Turbine (WT), a Fuel Cell (FC), Hydrogen Tank (HT), electrolyser, converter, and a Battery Storage (BS) back-up.

In addition, the Hybrid Optimisation of Multiple Energy Resources (HOMER) software coupled with Matrix Laboratory (MATLAB) software tool were selected for the simulation processes of the HRES. There are two sensitive variables that were inputted into the written codes and available HOMER tool. This was done in order to achieve an optimal result. The two sensitive variables are the PV tilt angle and the WT hub height. Hence, the effects of the PV tilt angle and WT hub height from the PV and WT systems have been infused into the system. By having knowledge of the load requirements of the selected LTE BTS site, two distinct configurations (PV/WT/FC/BS) and (DG/BS) simulation results have been compared, respectively. The simulation results clearly showed that in comparison to the DG/BS system, the proposed PV/WT/FC/BS HRES reduced the Net Present Cost (NPC), and GHG emissions by values of 40% and 100%, respectively. It was observed that the Capacity Shortage Fraction (CSF) was less than 1%, while the other important indicator such as the Renewable Fraction (RF) was increased by 100%. It is clear that the proposed HRES would improve the electric power supply to the LTE BTS at a reduced NPC and

acceptable GHG emissions, which in-turn, alleviates excessive costs and environmental effects from GHG emissions.

TABLE OF CONTENTS

LIST OF FIGURES

LIST OF TABLES

LIST OF ABBREVIATIONS

AC	Alternating Current
AGM	Absorbent Glass Mat
AT	Ambient Temperature
BS	Battery Storage
BTS	Base Transceiver Stations
CC	Cycle Charging
CI	Clearness Index
CSF	Capacity Shortage Fraction
DC	Direct Current
DG	Diesel Generator
FC	Fuel Cell
FGA	Fuzzy genetic algorithms
HRES	Hybrid Renewable Energy System
HT	Hydrogen Tank
LCC	Life-cycle cost
LF	Load Following
LTE	Long-Term Evolution
MATLAB	Matrix Laboratory
NASA	National Aeronautics and Space Administration
NOCT	Nominal Operating Cell Temperature
O&M	Operation and maintenance
OPEX	Operation Expenditure
PHS	Pumped Hydro Storage

PM	Particulate matter
QoS	Quality of Service
RER	Renewable Energy Resources
RES	Renewable Energy Sources
RF	Renewable Fraction
SI	Solar Irradiance
SMES	Super Magnetic Energy Storage Systems
SOC	State of Charge
STC	Standard Test Conditions
STP	Standard temperature and pressure
SV	Salvage value
TAC	Total Annualised Cost
UC	Ultra Capacitors
WE	Wind Energy
WP	Wind power
WS	Wind Speed
WT	Wind Turbine
BESS	Battery Energy Storage Systems
CAES	Compressed Air Energy Systems
COE	Cost of Energy
DPSP	Deficiency of Power Supply Probability
EENS	Expected Energy Not Served
ESS	Energy Storage Systems
FES	Flywheel Energy Storage

GA	Genetic Algorithms
HES	Hydrogen Energy Storage
HOMER	Hybrid Optimisation of Multiple Energy Resources
LCOE	Levelized cost of energy
LLP	Loss of Load Probability
LPSP	Loss of Power Supply Probability
NPC	Net Present Cost
PSO	Particle Swarm Optimisation
SA	Simulated Annealing
ACO	Ant Colony Optimisation
ANN	Artificial neural network
HO	Hybrid Optimisation
LM	Levenberg-Marquardt
MCS	Monte Carlo Simulation
PCA	Principal Component Analysis
RSM	Response Surface Methodology
TS	Tabu search
HOGA	Hybrid Optimisation by Genetic Algorithms
MIMO	Multiple-input and multiple-output
PA	Power amplifier
RMSE	Root Mean Square Error
SAO	Simulated Annealing Optimisation

NOMENCLATURE

N_{trx}	is the total number of transceivers
σ_{dc}	is a representation of the lost power in the rectifier in %
σ_{ac}	is a representation of the lost power in the cooling in %
σ_{ms}	is a representation of the lost power in the mains in %
P_0	is the static power
P_{out}	is the dynamic power (ranges from *zero* to P_{max})
Δp	is the load-reliant power consumption slope
Y_{PV}	Rated capacity of the PV under Standard Test Conditions in kW
f_{PV}	PV derating factor
G_T kW/m^2	Incident of solar irradiance on the PV array in the current time-step in
$G_{T,STC}$	Incident solar irradiance at standard test conditions in 1 kW/m^2
T_C	PV cell temperature of the in the current time-step in ◦C
$T_{C,STC}$	PV cell temperature under standard test conditions at 25 ◦C
α_p	Temperature coefficient of power in %/◦C
T_a	Ambient temperature in ◦C
$T_{a,NOCT}$	Ambient temperature at 20 ◦C at which the NOCT is defined
$T_{C,NOCT}$	Nominal Operating Cell Temperature in ◦C
$G_{T,NOCT}$	Solar irradiance at 0.8 kW/m^2 at which the NOCT is defined
τ	Solar transmittance of any cover over the PV array in %

$\eta_{mp,STC}$ Maximum power point efficiency under standard test conditions in %

α_{PV} PV array solar absorptance in %

H_{ave} Average monthly radiation on the horizontal surface of the earth in kWh/m^2/day

$H_{o,ave}$ Extraterrestrial horizontal radiation on a horizontal surface at the top of the earth's atmosphere in kWh/m^2/day

n Number of days of the year

$u(h_{an})$ WS at anemometer height in m/s

h Hub height of selected location

h_{an} Anemometer height in metres

α Power-law exponent

$P_{WT,\ STP}$ WT output power at STP in kW

ρ Actual air density in kg/m^3

P_{WT} WT output power in kW

ρ_0 Air density at STP (1.225 kg/m^3)

Δt Length of the time-step in hours

k Storage rate constant [h-1]

c Storage capacity ratio

Q Total amount of energy in kWh in the storage bank at the beginning of the time-step

Q_1 Available energy in kWh in the storage bank at the beginning of the time-step

Q_{max}	Total capacity of the storage bank in kWh
αc	Storage banks maximum charge rate at A/Ah
V_{nom}	Storage banks nominal voltage in volts
I_{max}	Maximum charge current of the BS in amperes
N_{batt}	Number of batteries in the storage bank
$\eta_{batt,c}$	Storage charge efficiency
P_{gen}	Electrical output of the generator in kW
Y_{gen}	Rated capacity of the generator in kW
F_1	Fuel curve slope in L/hr/kW
F_o	Fuel curve intercept coefficient in L/hr/kW
F	Fuel consumption rate in L/hr
$C_{anu,tot}$	Systems total annual cost in ZAR/yr
i_{dr}	Actual discounted rate annually in %
R_{pjt}	Lifetime of the project in years
CRF	Capital recovery factor
i	Real interest rate annually and
N	Number of years
R_{comp}	Component lifetime in years
C_{rep}	Replacement cost in $
R_{rem}	Remaining life of the component at the end of the project lifetime

R_{proj}	Project lifetime in years
R_{rep}	Replacement cost duration
INT()	Function that returns the integer amount of a real number
E_{srvd}	Total electrical load served in kWh/year
H_{srvd}	Total thermal load served in kWh/year
C_{boiler}	Boiler marginal cost in $/kWh
$CO_{2,E}$	Annual CO_2 emissions in kg/yr
$CO_{2,C}$	Cost of CO_2 emissions in $/t
UHC_E	Annual unburned hydrocarbons (UHC) emissions in kg/yr
UHC_C	Cost of UHC emissions in $/t
CO_E	Annual carbon monoxide (CO) emissions in kg/yr
CO_C	Cost of CO emissions in $/t
PM_E	Annual particulate matter (PM) emissions in kg/yr
PM_C	Cost of PM emissions in $/t
$SO_{2,E}$	Annual sulfur dioxide (SO_2) emissions in kg/yr
$SO_{2,C}$	Cost of SO2 emissions in $/t
NOx_E	Annual nitrogen oxide (NOx) emissions in kg/yr
NOx_E	Cost of NOx emissions in $/t
E_{cs}	Total annual capacity shortage in kWh/year

E_{dmd} Total electrical demand (primary and deferrable load) in kWh/year

H_{nren} Non-renewable thermal production in kWh/year

$E_{grid,sales}$ Energy sold to the grid in kWh/year (included in E_{served})

E_{nren} Non-renewable electrical production in kWh/year

CHAPTER ONE: INTRODUCTION

1.1. Background and Motivation

The telecommunication industry has encountered multiple difficulties with the ever-increasing user demands in terms of services such as voice, data, video conference, chatting, and social media, which in-turn puts pressure on the telecom companies to provide more infrastructure especially in the rural areas [1]. In South Africa for example, the lack of power for rural areas, power interruption and constricted infrastructure of the national grid are some of the critical hindrances the telecommunication operators are faced with, in the deployment of their networks [2]. In developed countries, such hindrances are readily overcome because of their well-developed grid infrastructure [2]. However, in a developing country like South Africa, where the grid connection is non-existent in the majority of the outlying rural areas, it is always hard to provide power supply to the Long-Term Evolution (LTE) Base Transceiver Stations (BTS) [3]. This is because there is a cost to the company as per the infrastructures required to connect the power from sources to the users who are diverse in terms of location, sparse population, low incomes, hence the need to be part of the global world. This presents a complication in developing countries like South Africa as mobile communication is increasingly expanding more and more into rural areas where access to the national grid is limited or non-existent [3]. The electrification by extension of the grid or secondary power station can only cover a small portion of the households in outlying rural areas [4]. Also, it is not cost-effective to extend the grid to such places due to the huge distance from developed regions [4].

The utilisation and implementation of Renewable Energy Resources (RERs) are rapidly increasing in developing countries and globally [5]. Consequently, the world is becoming less reliant on fossil fuels to lessen the effects of Greenhouse

Gas (GHG) emissions on the environment with the help of RERs [5]. Due to the increased global warming effects by GHG, there is an increased need to utilise emission-free energy solutions [6]. South Africa is endowed with natural and environmentally-friendly energy sources such as sunlight, winds and other natural resources that resulted in the abundance of RERs required for potential application and implementation of renewable energy technology in rural areas [6]. In addition to energy generation by RERs being environmentally-friendly, this has led to the reduction of the use of fuels and minor operating costs and the lessening of initial capital investment when compared to the conventional national grid infrastructures [7]. This, therefore, is very important for telecommunication operators and the deployment of LTE BTSs in rural areas [7]. LTE is the latest cellular network generation, simply termed fourth-generation network, which provides high data rate, support service convergence, huge bandwidth, easy upscale and small-sized equipment for easy deployment [8]. The deployment of such networks in the rural areas is inevitable due to easy homogeneous network demands, national telecommunication regulation demands, development of rural areas as economic hubs and advancement in services needed by cellular network users [8]. Thus, for powering LTE BTSs in rural or remote areas, different Renewable Energy Sources (RESs) need to be considered to obtain a reliable, affordable and efficient RES system that can easily meet the load demand of the LTE BTSs [9].

Designing a system that is reliable, efficient and that requires little or no maintenance and environmentally-friendly is crucial for powering an LTE BTS in remote areas [10]. Although it is possible to use one specific kind of RES, such as solar Photovoltaic (PV), to power an LTE BTS in a remote area, no power will be supplied during the night. This is because the PV is dependent on the sun to generate electricity. A hybrid system comprising of PV, Wind Turbine (WT), Fuel Cell (FC) and a Battery Storage (BS) is used to meet the LTE BTS load demand. This improves the supply of energy to the load. To increase the

reliability of the system, an energy storage system is added to store the excess energy generated by the RESs. This energy will be used to supply power to the load when the RESs are unable to meet the load demands [10]. The system described above is referred to as Hybrid Renewable Energy System (HRES) [11]. HRESs that have a combination of RES's and BS are preferred for powering LTE BTSs, especially in rural or remote areas [11].

1.2. Problem Statement

Due to the ever-increasing number of telecom subscribers, telecommunication operators are eager to broaden their network infrastructure as well as end-user service, this shows that there is need to consider other energy options such as RERs for powering the LTE BTS [12]. The rationale to deploy HRES as the primary RESs for the telecommunication sector in a developing country like South Africa is to stamp down the environmental effects of traditional energy sources, such as the DG that is commonly used as a back-up system for remotely located LTE BTS [12]. The deployment of an HRES can help mitigate pollutants coming from over-dependence on the national grid and diesel generators [13]. Furthermore, the benefit of incorporating a micro-grid HRES would ultimately reduce the high costs of maintenance and operation of the DG or coal-powered power plants [12]. In addition, this is going to enhance LTE BTS sites power supply stability [12]. In essence, the latest exploration into "green energy for communication" intends to ameliorate energy efficiency, bring down the Operation Expenditure (OPEX) as well as reduce GHG pollutants created by DG to improve the evolution of telecommunication [12]. Surprisingly, the electrical power expenditure from the LTE BTS is high in comparison to the rest of the networking OPEX [12]. The telecommunications sector, which provides video, voice, Internet and cloud services, has annually produced more than 830 million tonnes of carbon dioxide (CO_2) [12]. This equates to approximately 2% of the total global CO_2 emissions [12].

Hence, the deployment of sustainable energy resources, for instance, PV and Wind Power (WP) will assist with preventing these issues [13]. Moreover, there is the continual development of the cellular network in South Africa [14]. However, the electric power supply from the national grid is unreliable [14]. It is also noted that several LTE BTSs, as well as DG, are built-in residential areas [15]. In the course of a power outage or failure with the national grid, the DG instantly becomes operational. However, DG's are very noisy, which is not ideal for places like schools, hospitals as well as households occupants and their neighbours [16]. As a result, the deployment of PV and Wind Energy (WE) as a source of sustainable energy, in this particular case study, will help to enhance the electric power supply to the LTE BTS. Additionally, this will lead to a reduction of the effects of GHG emissions and noise on the environment. This can in due course reduce GHG emissions, improve the Quality of Service (QoS), as well as bring down OPEX for telecommunication companies in South Africa.

1.3. Aim and Objectives of the Study

The aim of this study is to optimally design an HRES that has the potential of generating electrical power that can adequately supply an LTE BTS in South Africa's rural areas.

Objectives:

The specific objectives of this study are to:

I. Reduce the Net Present Costs (NPC) incurred by the typical Diesel Generator (DG)/BS system used to power the LTE BTS in rural areas;
II. Reduce the GHG emissions emitted by the DG/BS system that powers the LTE BTS in rural areas and

III. Optimise the HRES considering (i) and (ii) above and reliability of the entire system.

1.5. Thesis Outline

Chapter 2.

In this chapter, the application and the feasible modelling methods for different RERs and RESs (PV, WT and FC systems) used in the proposed HRES are reviewed. Also, the preferred lead-acid batteries, lead-acid batteries modelling methods and energy storage methods are reviewed. The HRESs controlling methods for powering the LTE BTS load are reviewed with a particular highlight around ensuring the maximum lifetime of the battery which involves the charging and discharging of the battery. Finally, the optimisation methods are discussed, focussing on the Hybrid Optimisation Model for Electric Renewables (HOMER) software, for the reason that it is the preferred optimisation tool widely used in the industries for all such simulations related to the HRES.

Chapter 3.

Presented in this chapter is the methodology employed in the optimisation tool as well as the algorithm used to verify the result. The chapter details the study areas, the collection of climatic data sets needed for this optimisation problem, the profile of the load, pre-processing and modelling of the data. The modelling methods for the power generated by each of the RES's are discussed as well as the modelling method for the insertion of the BS into the system. The presumptions and strategies utilised for preparing the HOMER software are reviewed in-depth with regard to the objective function of the NPC and GHG emissions of the system. In the end, the control algorithm utilised to authenticate the HOMER software results is described.

Chapter 4.

In this chapter, the results obtained from the modelling, sizing and simulation are discussed. All the feasible configurations presented by the simulation results are compared according to the stipulated objectives and constraints, to see which is the most feasible, cost-effective, reliable and environmentally-friendly HRES between the proposed PV/WT/FC/BS HERS and the DG/BS system that is currently utilised to power LTE BTSs in the rural areas.

Chapter 5.

Conclusion and Recommendations: The results and findings from chapter 4 are concluded and the main findings of the project are highlighted together with future recommendations.

1.6. Publications

The publications below are materials forming part of this dissertation.

- S. T. Leholo, P. A. Owolawi, and K. T. Akindeji, “Modelling and Optimisation of Hybrid RE for Powering Remote GSM Base Station,” 2018 IEEE PES/IAS PowerAfrica, Nov. 2018.
- S. T. Leholo, P. A. Owolawi, and K. T. Akindeji, “Performance Analysis of a Hybrid Micro-Energy System for SA Data Centers,” E3S Web of Conferences, vol. 64, p. 01003, 2018.
- S. T. Leholo, P. A. Owolawi, and K. T. Akindeji, “Solar Energy Potential Forecasting and Optimisation Using Artificial Neural Network: South Africa Case Study,” 2019 Amity International Conference on Artificial Intelligence (AICAI), 2019.

CHAPTER TWO: LITERATURE REVIEW

LTE BTSs that are situated in inaccessible or remote areas need a power source that is reliable and efficient [17]. These will allow for uninterruptible and continuous service to the end-user [17]. Since most of the LTE BTSs that are situated in inaccessible or remote areas are not connected to the national grid, HRESs are found to be very promising in helping with such an issue [17]. Optimisation of these HRESs is a crucial factor when designing a system that can meet the load demand of the LTE BTSs situated in inaccessible or remote areas [18]. The optimisation of an HRES for the LTE BTS focuses on the optimal sizing of the components of the HRES so that the LTE BTS can be supplied a power supply that is reliable, cost-effective, efficient, and environmentally-friendly [18]. When optimising an HRES, it is very crucial to choose the correct component to be part of the HRES [19]. Furthermore, it is crucial to select RESs that can perform optimally for a particular case [20]. In the process of optimising an HRES, numerous objectives can be considered that the optimised HRES must fulfil [20]. These objectives can include minimising the costs of the system and improving the efficiency of the system [21]. In the past years, there have been several optimisation methods that have been proposed by various authors for the optimisation of HRESs. In this chapter, the different optimisation methods that have been utilised in different studies for optimisation of HRESs will be reviewed and compared to highlight their strengths and weaknesses.

2.1. Optimisation Methods for Hybrid Renewable Energy Systems

The optimisation techniques and methods can help to optimise the HRES according to the objectives defined [20]. In literature, there are plenty of methods that can be used for the optimisation of HRESs [21]. Some of these methods take a heuristic approach and others take a gradient-based optimisation approach [20]. Some of the commonly used methods reviewed in the literature

are software tools, Ant Colony Optimisation (ACO), Hybrid Optimisation (HO), Simulated Annealing Optimisation (SAO), Particle Swarm Optimisation (PSO), Fuzzy Genetic Algorithms (FGA), and Genetic Algorithms (GA) [20].

2.1.1. Genetic Algorithms Optimisation Method

The GA is an algorithm that is evolutionary population-based and includes multiple operations such as selection, crossover, mutation, and initialisation that ensure that an optimal solution to a specific problem is obtained. This method can solve problems by utilising multiple solutions but can be stuck in local minima if it is not initialised or designed properly. In literature, multiple studies have utilised the GA to optimally size an HRES for remote or rural applications. Table 2.1-2.2 show several studies in the literature review where the GA optimisation method has been applied.

Table 2. 1. Studies where the GA optimisation method was applied.

Reference	Goal	Results
Addoweesh et al [23]	The GA was used for a techno-economic analysis for a small hybrid system to meet the load demand of a remote village in Saudi Arabia.	It was found that the inclusion of batteries reduced the required DG.
Chen et al [24]	The adaptive GA was used to determine the optimum capacity of an off-grid hybrid energy system considering reliability and cost.	A higher capacity of RESs increases the installation cost and reduces the CO_2 emissions coming from DG.

Table 2. 2. Studies where the GA optimisation method was applied.

Reference	Goal	Results
Berger et al [25]	The GA was used for the optimisation of a stand-alone PV/WT/DG HRES with different BS technologies for a telecommunication site in Syria.	The use of BS combined with the RESs is ecological and economical.
Ndongo et al [26]	The GA was used to determine the optimal size of an off-grid PV/WT HRES for two places in Senegal.	The optimal configuration was PV/WT/BS HRES by the use of the first load profile. Furthermore, 64% and 71% of energy come from the WT on the two sites.
Fahmy et al [27]	The GA was used for the optimal economical sizing of a PV/WT HRES for Water Irrigation in Sinai, Egypt.	The PV/WT HRES and PV stand-alone system are the most suitable than the other systems for the selected sites.

2.1.2. Particle Swarm Optimisation Method

The PSO simulates the social behaviour of how a swarm moves to find food in a specific area. The PSO optimises a problem by iteratively trying to improve a candidate solution for a given objective function. The PSO is efficient in solving the optimisation and scattering problems. However, multiple modifications are required by this method due to its conflicted and complex nature. In literature, multiple studies have utilised the PSO to optimally size an HRES for remote or

rural applications. Table 2.3-2.4 show several studies in the literature review where the PSO optimisation method has been applied.

Table 2. 3. Studies where the PSO method has been applied.

Reference	Goal	Results
Chaabene et al [28]	The PSO was used for the optimisation of a PV/DG/BS HRES for a typical house in Tunisia.	The cost of the system optimised using minimum pollution criterion has about 0.3% extra overall cost compared to the system optimised using minimum overall system cost criterion.
Benbouzid et al [29]	The PSO was used for the optimisation of a PV/WT//Tidal/BS HRES for a remote area in Bretagne, France.	The best results in the area under study is a WT/BS system and the solution is dependent on multiple variables such as electric load demand and weather data.
M'Sirdi et al [30]	The PSO was used for the optimisation of an HRES to meet the load demand of a typical house.	The PSO proved its high sensitivity and intensity in solving such optimisation problems.

Table 2. 4. Studies where the PSO method has been applied.

Reference	Goal	Results
Alolah et al [31]	The PSO was used for the optimisation of a PV/WT//DG/BS HRES for remote areas in Saudi Arabia.	The simulation results affirmed that PSO is a promising optimisation technique.
Dwivedi et al [32]	The PSO was used for the optimal sizing of a stand-alone PV/WT/Hydro/Biomass HRES for village hamlets of the Indian state of Uttarakhand.	The third scenario PV/WT/Hydro/Biomass HRES offers minimum total annual cost.

2.1.3. Simulated Annealing Optimisation Method

SAO is based on the annealing process in metallurgy where a piece of metal is melted at a very high temperature then is cooled down and at the end is frozen into a crystalline state with the least amount of energy. The metal in this process results in the development of crystal sizes that are larger with fewer defects in the structure of the metal. The SA method guarantees to find an optimal solution because it can deal with non-linear models statistically. However, this method requires quite many initial constraints. In literature, multiple studies have utilised the SA to optimally size an HRES for remote or rural applications. Table 2.5 shows several studies in the literature review where the SAO method has been applied.

Table 2. 5. Studies where the SAO method has been applied.

Reference	Goal	Results
Varun et al [33]	The SAO was used for sizing analysis and cost optimisation of a PV/DG/BS HRES for a residential colony of 135 houses in Moradabad district, India.	The optimised PV/DG/BS HRES has the least Life-Cycle Cost (LCC), CO_2 emissions and annual diesel consumption in comparison to older models.
Ekren et al [34]	The SAO was used for the optimisation of a PV/WT/BS HRES for a campus area in Turkey.	The SA algorithm gives better results in comparison to the Response Surface Methodology (RSM).
Nayar et al [35]	The SAO was used for the optimisation of a hybrid DG/BS energy system for remote communities.	A considerable saving on the running cost is achieved by the hybrid energy system in comparison to DG only system.

2.1.4. Ant Colony Optimisation Method

The ACO method is based on the behaviour of ants when they utilise a specific pheromone for marking the pathway for the rest of the colony. The method allows the colony to use the shortest distance that leads to food. This behaviour by the ants is simulated by the ACO to determine the optimal solution for a certain or provided objective function. The ACO method has a high convergence speed but requires a long-term memory space. In literature, multiple studies have utilised the ACO to optimally size an HRES for remote or rural applications. Table 2.6 shows several studies in the literature review where the ACO method has been applied.

Table 2. 6. Studies where the ACO method has been applied.

Reference	Goal	Results
Mittal et al [36]	The ACO was used for optimal sizing of a PV/WT HRES for a village in the central region of India – Madhya Pradesh.	The optimally sized configuration of the proposed HRES is found to provide excellent performance with less energy cost and reduced unmet load.
Vijay et al [37]	The ACO was used for the optimal placement and sizing of a PV/WT HRES.	The ACO algorithm is superiority and provides an idea for solving complex Indian practical generating systems.
Askarzadeh et al [38]	The ACO was used to optimally size a PV/WT/BS HRES for having a reliable system.	It is observed that ACO yields more promising results than the other studied methodologies.

2.1.5. Hybrid Optimisation Method

The HO method combines two or more optimisation methods that can overcome the limitations of using a single optimisation method. This method provides a more reliable and effective solution for the optimisation of HRESs. Although the HO method improves the overall performance of the optimisation, the method suffers from premature convergence when it deals with complex optimisation problems. In literature, multiple studies have utilised the HO to optimally size an HRES for remote or rural applications. Table 2.7 shows several studies in the literature review where the HO method has been applied.

Table 2. 7. Studies where the HO method has been applied.

Reference	Goal	Results
Ameri et al [39]	The Monte Carlo Simulation (MCS) Method and PSO Algorithm were used for optimal sizing of a stand-alone HRES for powering an off-grid remote area located in Rafsanjan, Iran.	The WT/BS system is the most cost-effective for different months of the year and the MCS Method can provide a novel approach to the tools already present in the field of optimisation.
Karapidakis et al [40]	The SAO and tabu search (TS) methods were used for optimal sizing of an autonomous power system with renewables.	The hybrid SA-TS improved the obtained solutions, in terms of convergence and quality, in comparison to the solutions provided by individual TS or SA method.
Sopian et al [41]	The iterative and GA method was used for the optimisation of a PV/WT micro-grid for rural housing electrification in Kuala Terengganu, Malaysia.	By applying the monthly optimum tilt angle, the collected yields of the PV array increased by as much as 7.96%.
et al [42]	The artificial neural network (ANN) and GA method were used for the optimal sizing of a stand-alone PV system.	The proposed exponential regression model with three coefficients presents more accurate results than the conventional regression models.

2.1.6. Software Tools Optimisation Method

There are several common software tools commonly utilised by researchers and engineers around the globe [43]. These tools are commonly utilised to design and evaluate the hybrid micro-grid system feasible performance [43]. Through the utilisation of the simulation and optimisation software, the optimum configuration of the designed hybrid micro-grid system can be attained [43]. This is achieved through the comparison of the energy production cost and performance of several configurations of the hybrid micro-grid system [43]. Table 2.8-2.9 show the demerits and merits of the several simulation software tools utilised in today's world when it comes to the optimisation of HRESs [43]. Table 2.10-2.12 shows several studies in the literature review where these simulation software tools have been applied.

Table 2. 8. The strengths and weaknesses of the various simulation software.

Software	strengths	weakness
HOMER	This tool has hourly data handling capacity, provides an efficient graphical representation of results, easy to understand and user friendly.	In this tool, the time series data in a form of daily average cannot be imported, and reliability analysis cannot be performed.
RETScreen	This tool is easy to use as it is EXCEL based software, financial analysis is the main strength, meteorological database from NASA only and strong product database.	The tool lacks some time series data import options, has less data input options, has limited options for search, retrieval, and visualisation features.

Table 2. 9. The strengths and weaknesses of the various simulation software.

Software	strengths	weakness
HYBRID2	The tool has a detailed dispatching option, multiple electrical load options, and is user friendly.	The tool does not work on windows platforms later than WindowsXP.
Hybrid Optimisation by Genetic Algorithms (HOGA)	This tool requires low computational time and has a capability of sensitivity analysis and mono or multi-objective optimisation.	Internet connection is required to activate the tool licence, and the free educational version comes with analysis limitations.

Table 2. 10. Studies where the software tools have been applied.

Reference	Goal	Results
Yaïci et al [44]	The RETScreen tool was used for cost and feasibility analysis of a PV/Biomass hybrid energy system in off-grid areas of Bangladesh.	The results showed the proposed system is more environmentally-friendly, less costly and reliable than the conventional kerosene-based system.
Warner et al [45]	The HYBRID2 tool was used for modelling a PV/WT/DG HRES in South American.	The predicted performance discrepancies are due basically to different subcomponent models and differences in the control strategy.

Table 2. 11. Studies where the software tools have been applied.

Reference	Goal	Results
Guzman et al [46]	The HOGA tool was used for the optimisation of a PV/DG hybrid energy system to power the 'La mansion' hotel in the town of Acacias, Meta (Colombia).	The combination of DG and PV is a good alternative to meet lighting power demand in the hotel 'La Mansion', even in night hours thanks to the BS.
Hazelton et al [47]	The HOMER tool was used for the optimisation of a PV/DG/BS hybrid energy system for a case study in Sabah, Malaysia.	The presence of RESs improves the performance of stand-alone systems and reduces energy storage requirements.
Ramli et al [48]	The HOMER tool was used for the environmental and techno-economic feasibility of a PV/DG/BS hybrid energy system to supply electricity for a remote rural village in Iraq.	The sensitivity analysis of ambient temperature demonstrated that the PV and batteries are highly affected by an increase in temperature.
Fransson et al [49]	The TRNSYS tool was used for the optimisation of a PV/WT/DG/BS hybrid energy system to provide electricity and drinkable water for two locations in Kenya and Sudan.	The optimised system has significant mitigation of environmental issues compared to using only diesel engines that are a common solution in disaster situations.

Table 2. 12. Studies where the software tools have been applied.

Reference	Goal	Results
Huda et al [50]	The HOMER tool was used for the optimisation of a PV/WT/DG hybrid energy system for a remote located mobile BTS station in Nigeria.	The optimised hybrid energy systems can significantly minimise the power generation cost and decrease CO_2 emissions when compared to the traditional DG only system.
Das et al [51]	The HOMER tool was used for the optimisation of a WT/DG hybrid energy system to support a small community.	The proposed system is suitably feasible with respect to the net present cost (NPC) and CO_2 emission reduction purpose.
Abdulateef et al [52]	The HOMER tool was used for the optimisation of PV/WT/DG hybrid power generation system in the rural area in Muqdadiyah district of Diyala state, Iraq.	RESs perhaps replace the conventional energy sources and would be a feasible solution for the generation of electric power at remote locations with a reasonable investment.
Ali et al [53]	The HOMER tool was used for the optimisation of a PV/WT hybrid energy system for a remote located mobile BTS station in Odisha, India.	The optimised system reduces the operating expenses as well as COE when compared with conventional DG only systems.

2.2. Summary of Literature Review

The literature reviewed has provided an overview of the various designs of hybrid systems, and optimisation methods that can be employed for optimisation of HRESs. One of the key findings is that an off-grid RES is a viable alternative to conventional fossil fuel or grid supply for supplying reliable power to rural or remote areas [49]. Combing to two or more RES's has shown to be an important method that can reduce costs and improve the reliability of RESs regardless of the intermittency that comes with RERs like SI and WS [52]. Furthermore, the incorporation of proper energy storage to the RES has clearly shown to improve the reliability of RESs in providing power to the load [52]. The optimisation of an HRES is not an easy undertaking. The components of the HRES have to be optimally sized for the feasibility of the system in terms of reliability and cost [50].

Based on the literature review, it has been found that LTE BTSs situated in remote or rural areas are not connected to the national grid and rely mostly on the DG as a source of power [50]. Even though there has been a considerable amount of research in the literature about the optimal sizing of HRES for rural or remote application, most of the optimally sized HRESs in the literature relied on the DG as a source of power or back-up. It has been found that these DG's are affected by various parameters, such as O&M costs, the fuel conversion efficiency of the generator, the price of fuel, renewable penetration, the capacity of the generator and BS [50]. Furthermore, these DG's are found to have some drawbacks which include [53]:

- DG's can make a lot of noise when running.
- DG's produce GHG emissions that are released into the environment.
- DG's have constant running cost due to filter changes, cleaning, and fuel.

- DG’s are also unreliable and often require expensive overhauls to be repaired.

- DG’s are expensive to run over the long-term.

Based on the drawbacks of using DG as a source of power or back-up, the objective of this work is to optimally design an HRES that has the potential of generating electrical power that can adequately supply an LTE BTS while at the same time reducing NPC and GHG emissions that come with using DG’s as a power source or back-up for LTE BTS in rural areas. The system performance under this work is compared with the existing DG powered LTE BTS in rural areas. Furthermore, from the literature, it has been discovered that HOMER software is the most widely used optimisation and simulation tool and provides an efficient graphical representation of results when it comes to the optimal sizing of HRESs. So in this study, HOMER software has been selected for the optimisation and simulation of the proposed HRES based on its capabilities. To the best knowledge of the authors, this is the first study investigating the use of FC as part of an HRES that can power an LTE BTS in rural areas of South Africa.

CHAPTER THREE: RESEARCH METHODOLOGY

This chapter outlines the methodology used in this study. The chapter is partitioned into five sections which are:

- Site Assessment -This section outlines the chosen sites and their analysis.
- RER Data Assessment - This section analyses the RERs data of the chosen sites.
- Load Analysis - This section outlines the chosen load and its load profile analysis.
- Proposed System - This section details the architecture of the proposed HRES and its components.
- Optimal Sizing Method - This section outlines the optimisation method used, mathematical models of the components of the HRES, specifications and costs of the components, parameters of the optimisation method and system operational control.

3.1. The Study Area

Six (6) rural sites in the North West province of South Africa, as shown in Figure 3.1, were chosen as the locations where the LTE BTSs are situated. The geographical data of these sites were used for the optimisation of the proposed HRESs used for powering these LTE BTSs. The six sites are Mafikeng, Lichtenburg, Rustenburg, Klerksdorp, Potchefstroom and Vryburg. These sites possess adequate SI and WS densities, and their selection was based on the fact that they are widespread throughout the North West province for generalisation of the final results of this study. The atmospheric characteristics and the population statistics of the selected sites are presented in Table 3.1.

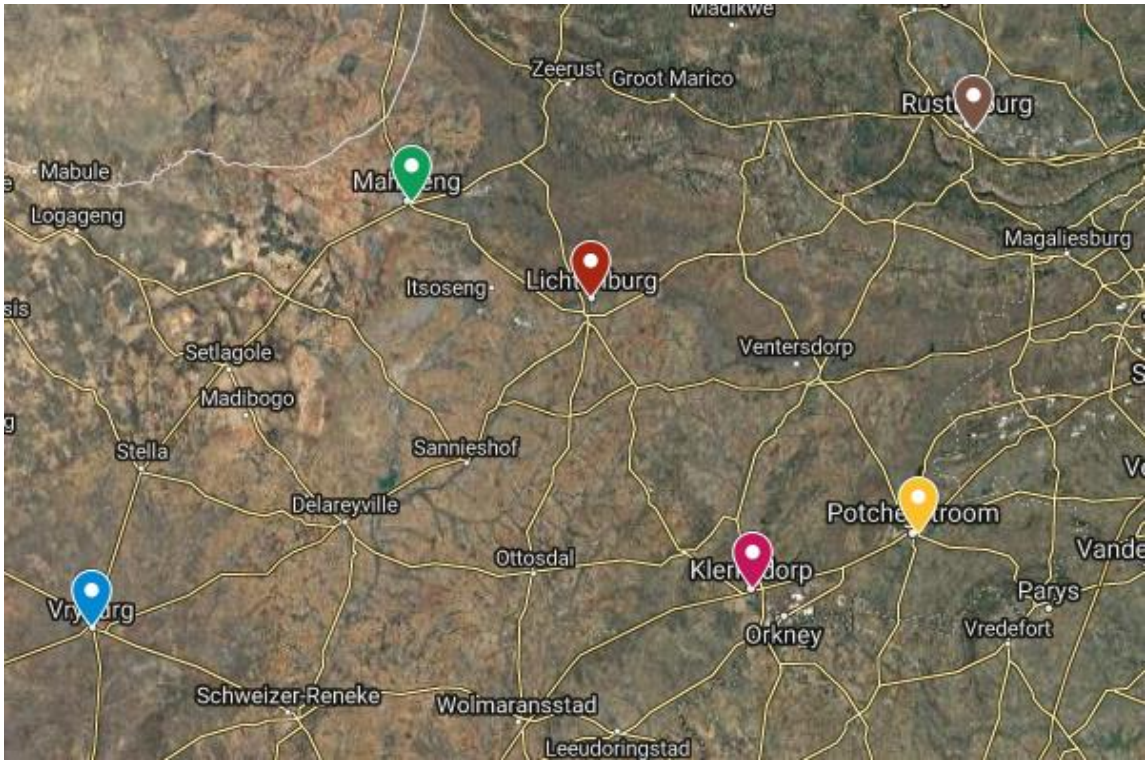

Figure 3. 1. Map of Rural Communities in North West [54].

Table 3. 1. Geographical data for each rural site.

Province	Latitude (South)	Longitude (East)	Area (km^2)	Elevation (m)	Population
Mafikeng	25.87°	25.64°	24.57	1500	49 300
Rustenburg	25.67°	27.24°	282.42	1170	549 575
Potchefstroom	26.72°	27.10°	162.44	1340	43 448
Vryburg	26.96°	24.73°	64.24	1194	48 200
Lichtenburg	26.11°	26.17°	108.90	1503	26 338
Klerksdorp	26.86°	26.63°	105.98	1318	178 921

3.2. Data Collection

Some specific data was required to be able to carry out this study. This data includes the site geographical position, Solar Irradiance (SI), Wind Speed (WS), Clearness Index (CI), Ambient Temperature (AT) and the electrical load profile of the LTE BTS. The average monthly SI, WS, CI and AT data used in this work was obtained from the National Aeronautics and Space Administration (NASA) Prediction of Worldwide Energy Resources database [55]. The duration of the data acquired from the NASA database was from 01/01/2019-31/12/2019. It ought to be mentioned that the NASA database was chosen because the satellite data has global coverage and provides reliable meteorological and solar resource data in sites where ground data measuring meteorological stations are sparse or non-existent [55]. The average monthly SI, WS, AT and CI data of the six chosen locations are presented in Figure 3.2-3.7.

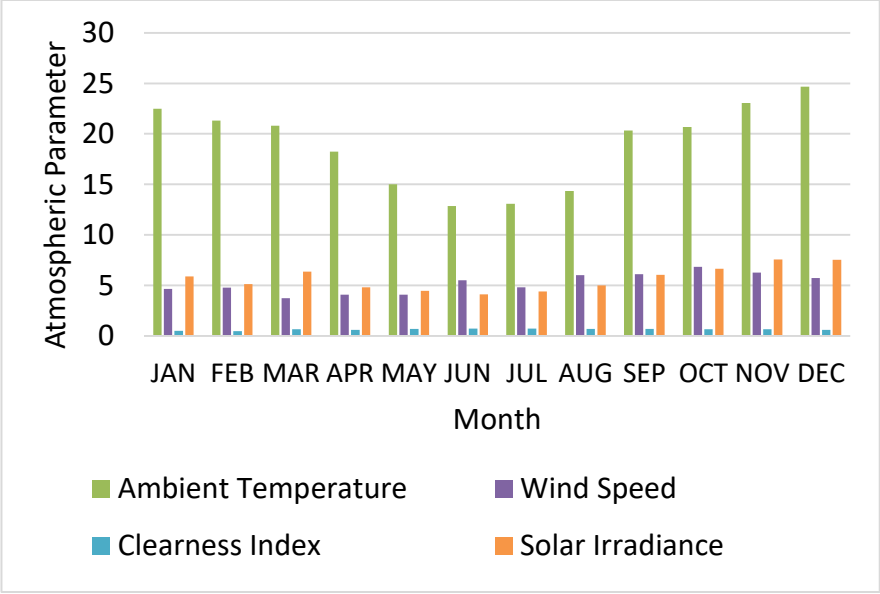

Figure 3. 2. Monthly variations of atmospheric parameters in Mafikeng.

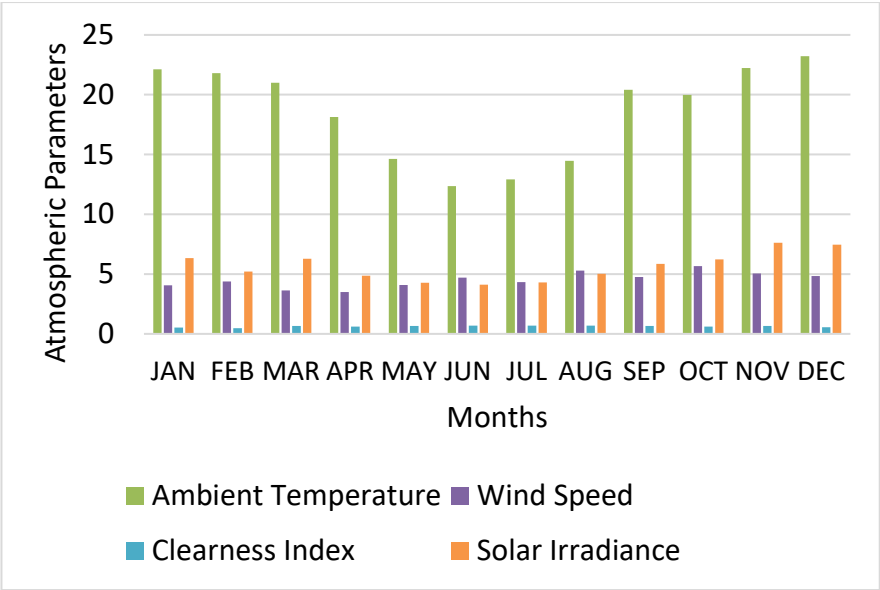

Figure 3. 3. Monthly variations of atmospheric parameters in Rustenburg.

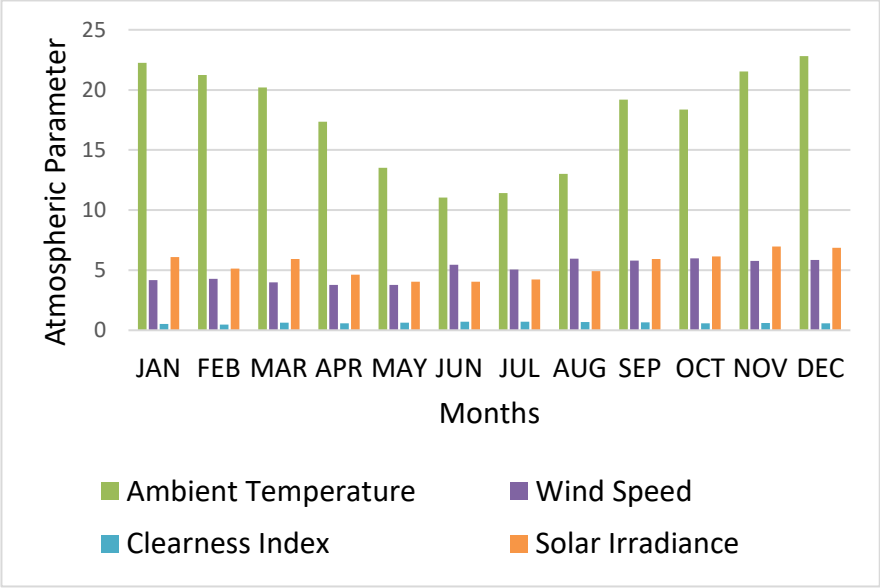

Figure 3. 4. Monthly variations of atmospheric parameters in Potchefstroom.

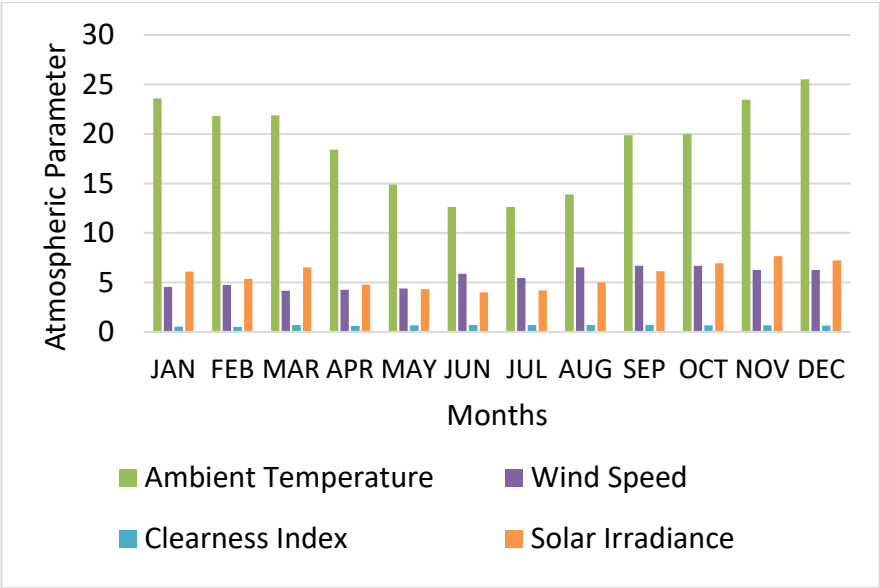

Figure 3. 5. Monthly variations of atmospheric parameters in Vryburg

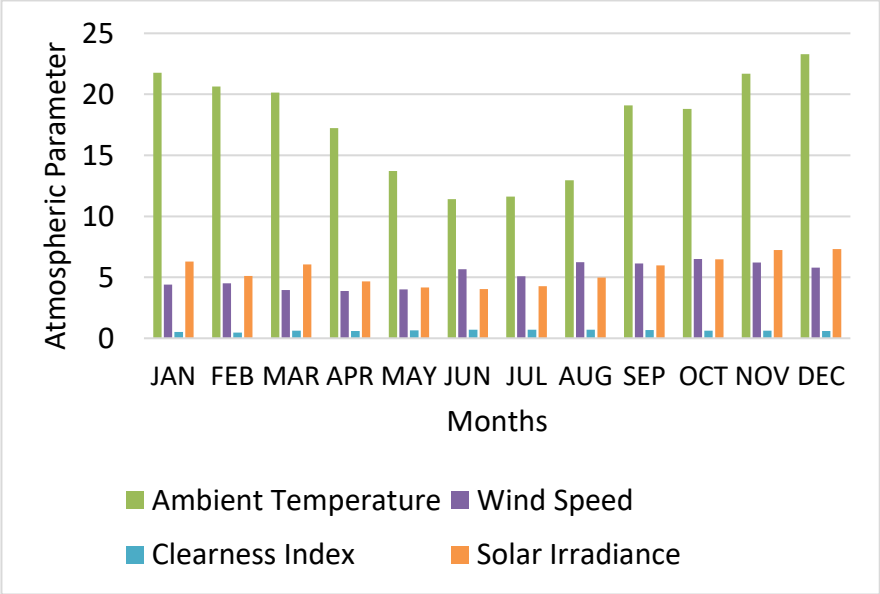

Figure 3. 6. Monthly variations of atmospheric parameters in Lichtenburg.

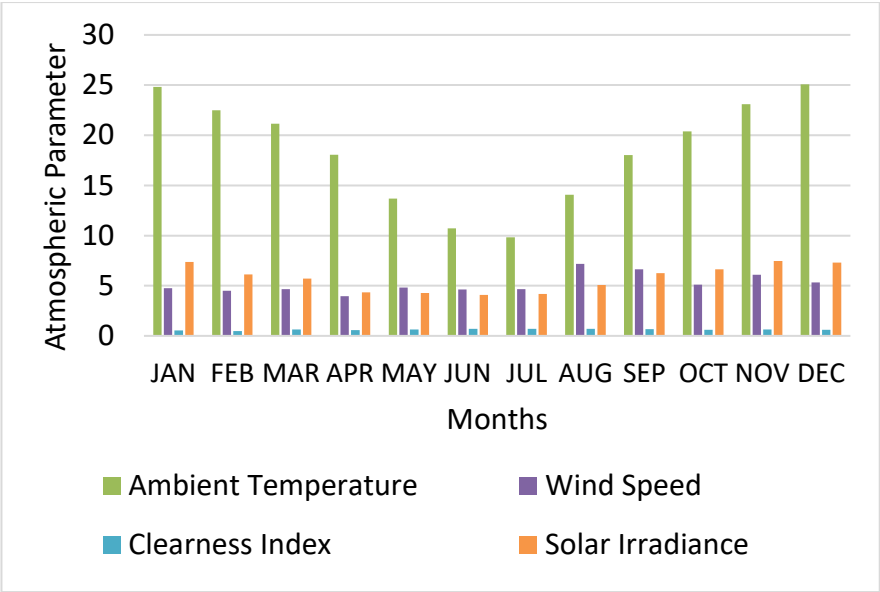

Figure 3. 7. Monthly variations of atmospheric parameters in Klerksdorp.

Table 3.2 presents the annual averages of the atmospheric parameters of all the chosen sites.

Table 3. 2. Annual averages of the atmospheric parameters.

Parameter	Mafikeng	Rustenburg	Potchefstroom	Vryburg	Lichtenburg	Klerksdorp
AT	18.90	18.61	17.66	19.04	17.7	18.45
WS	5.21	4.53	4.98	5.48	5.20	5.19
CI	0.63	0.63	0.62	0.64	0.63	0.63
SI	5.65	5.63	5.41	5.68	5.54	5.73

Furthermore, it is very important to show the correlation between all the atmospheric parameters to see the effects that each parameter has on each other. Since the annual averages of the atmospheric parameters of the different sites are very close to each other, only the correlation results of one site will be presented. Table 3.3 shows the correlation matrix of the atmospheric parameters of Mafikeng which was obtained. From the correlation table, it can be noted that the AT and WS have a huge positive correlation to the SI. This

means that the AT and WS have an effect on the amount of SI that can be attained in any chosen location. In the case of the AT, the CI has a huge negative correlation on the AT. This, therefore, means that a rise in the CI leads to a decrease in the AT and vice versa.

Table 3. 3. Correlation matrix of the atmospheric parameters of Mafikeng.

Parameter	AT	WS	CI	SI
AT	1	0,17	-0,60	0,87
WS	0,17	1	0,21	0,45
CI	-0,60	0,21	1	-0,18
SI	0,87	0,45	-0,18	1

An extensive pre-feasibility analysis was done for the effective as well as reputable designing of the HRES. Furthermore, the energy profile of the LTE BTS was crucial for the optimal sizing of the HRES to adequately power a rural LTE BTS.

3.3. Load Profile of the LTE BTS

In order to determine the power consumption and hourly load profile of the chosen LTE BTS, the architecture and the power consumption of the parts of these systems need to be explored. The mobile stations are connected to a core network through the BTS, which acts as an access link. A cell that is divided into multiple sectors is covered by these stations, with a sector antenna covering each sector [66] as demonstrated by Figure 3.8. The macro, micro, femto (indoor), and pico terms are used for classification of LTE BSs in accordance with their coverage area, with each cell having a distinct output power, size, and data rate [66]. When compared to their predecessors, modern LTE BTSs (eNBs) necessitate comparatively for lesser energy [66]. The tri-sectoral LTE BTS has a range of 500 m and is able to encapsulate a vicinity of approximately 0.66 km^2.

For rural/suburban districts, this encapsulation could increase to 7.8 km^2 [28]. The required power to manage fourth-generation cellular network in most cases is a couple of kW which differs with different LTE BTS designs. The power consumption by distinct designs of LTE BTSs like the micro, macro, femto and pico was quantified by the EARTH project [56].

Static and dynamic power consumptions are often used to describe the LTE BTS power consumption. The dynamic fluctuates with the quantity of deployed transceivers and traffic-load, while the static continues to be fixed. The authors in [67] provide valuable knowledge into the LTE BTS static and dynamic power consumption. According to the EARTH report, the components that consume power in an LTE BTS are the DC power supplies, power amplifier (PA), the baseband (BB) unit including the losses that occur in the feeder, radio frequency (RDF) module, cooling, and main power supply losses (mains).

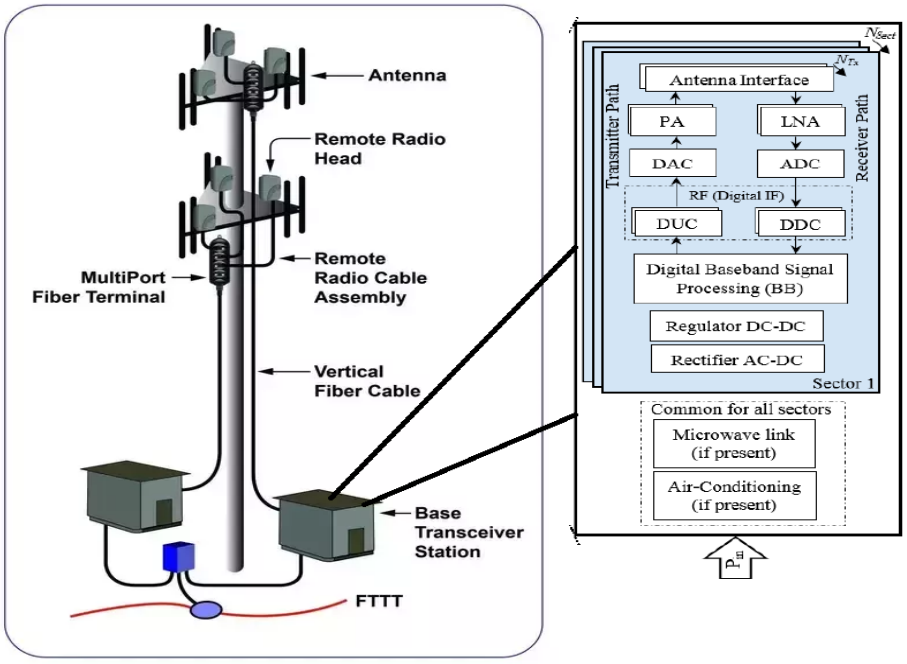

Figure 3. 8. Block diagram of the components in an LTE BTS [56].

When the sum of transceiver chains (N_{trx}) increases, it also causes the LTE BTSs power consumption to proportionally increase. This process may be expressed as [56]:

$$P_{bs} = N_{trx} \frac{P_{PA}+P_{BB}+P_{RF}}{(1-\sigma_{dc})(1-\sigma_{ac})(1-\sigma_{ms})}, \quad (3.1)$$

where

N_{trx} is the total number of transceivers, σ_{dc} is a representation of the lost power in the rectifier in %, σ_{ac} is a representation of the lost power in the cooling in %, and σ_{ms} is a representation of the lost power in the mains in %. At optimum load, for three precinct coverage individually possessing two multiple-input and multiple-output (MIMO) arrangement transceivers, the power consumption by the LTE BTS is discovered to be around 1.350 kW. The power consumption is different for various designs of mobile LTE BTSs. Table 3.4 shows the power consumption values of different kinds of BTSs. Each BTS type is depicted against the power consumption for each component of an individual transceiver chain. These include, for example, the consumption incurred by cooling, DC-DC power supply, and mains. The total power consumption is shown in the last column of Table 3.4. This power is equivalent to the power consumed by an individual transceiver chain multiplied by the total amount of transceivers.

Table 3. 4. Power consumption breakdown for various kinds of BTSs [56].

BTS Kind	NT RX	RDF (W)	PA (W)	DC-DC (W)	BB (W)	Mains (W)	Cooling (W)	Total per T_{rx} (W)	Total for $N_{T\,RX}$ (W)
Macro	6	12.9	128.2	16.88	29.6	20.25	22.5	225.0	1350
RRH	6	12.9	64.4	9.44	29.6	11.32	0.0	125.8	754.8
Micro	2	54	6.3	28.20	2.6	6.51	0.0	72.3	144.6
Pico	2	6.8	0.13	0.32	4.0	0.81	0.0	7.3	14.7
Femto	2	0.6	1.1	0.47	2.5	0.57	0.0	5.2	10.4

Equation (3.2) demonstrates the LTE BTS power consumption as a function of transceivers/traffic-load:

$$P_{bs} = N_{trx} \times \left(P_0 + \Delta_p P_{out}\right), (0 < P_{out} \leq P_{max}), \tag{3.2}$$

where

P_0 is the static power, P_{out} is the dynamic power (ranges from *zero* to P_{max}), and Δp is the load-reliant power consumption slope.

Equations (3.1) and (3.2) were used to determine the power consumption of the chosen LTE BTS [56]. The chosen LTE BTS has six transceivers and the P_{max} per transceiver is 20 W, then the maximum LTE BTS power consumption value at full traffic-load will be 1344 W, and a nominal value 780 W for zero traffic. Because air conditioning is crucial for an LTE BTS, 1 kW has been added to these values. On that basis, the consumption of power by the LTE BTS, consequently, varies between 1.8 kW at zero traffic-load and 2.35 kW at max load. These fundamental estimations offer the values that can be used to model an LTE BTS hourly load profile. The daily load profile of typical LTE BTS is shown in Figure 3.9. As seen in Figure 3.9, the LTE BTS daily energy

consumption is approximately 56 kWh/day with a peak demand of around 2.35 kW.

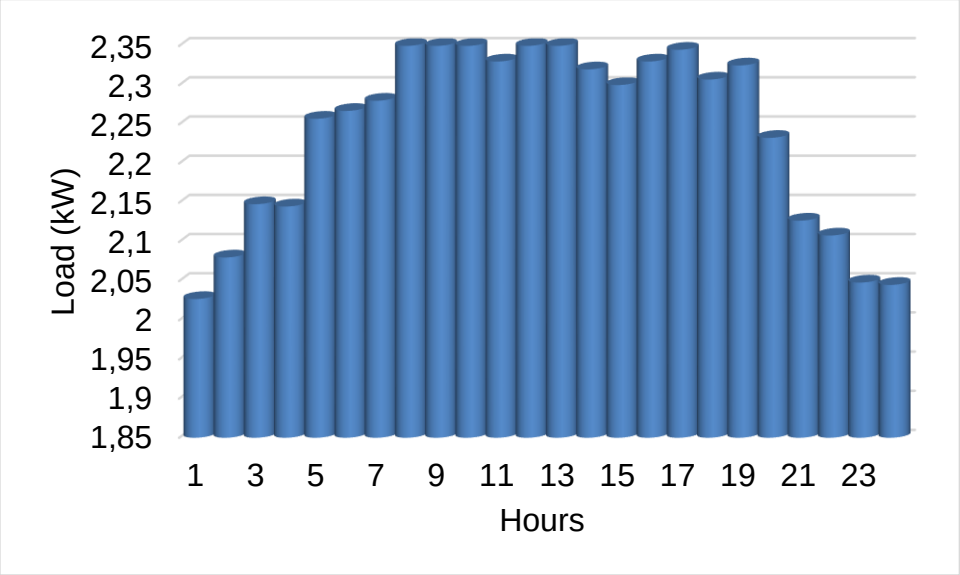

Figure 3. 9. Typical LTE BTS load profile.

3.4. Experimental Setup

This section presents the architecture and experimental setup of the proposed HRES. Shown in Figure 3.10 is the typical setup of a telecom BTS powered by an HRES in Kenya [57]. Figure 3.11 shows the schematic diagram of the proposed HRES system, which includes three main power sources (PV, WT and FC) connected in parallel. The selection of this configuration was done based on the facts that:

- The design of this kind of systems is ideal for rural areas; they increase the reliability of the system and also to lessen the fuel costs associated with DG.
- The configuration of this kind allows for separate or simultaneous operation of the input sources.

Figure 3. 10. A telecom BTS powered by an HRES in Kenya [57].

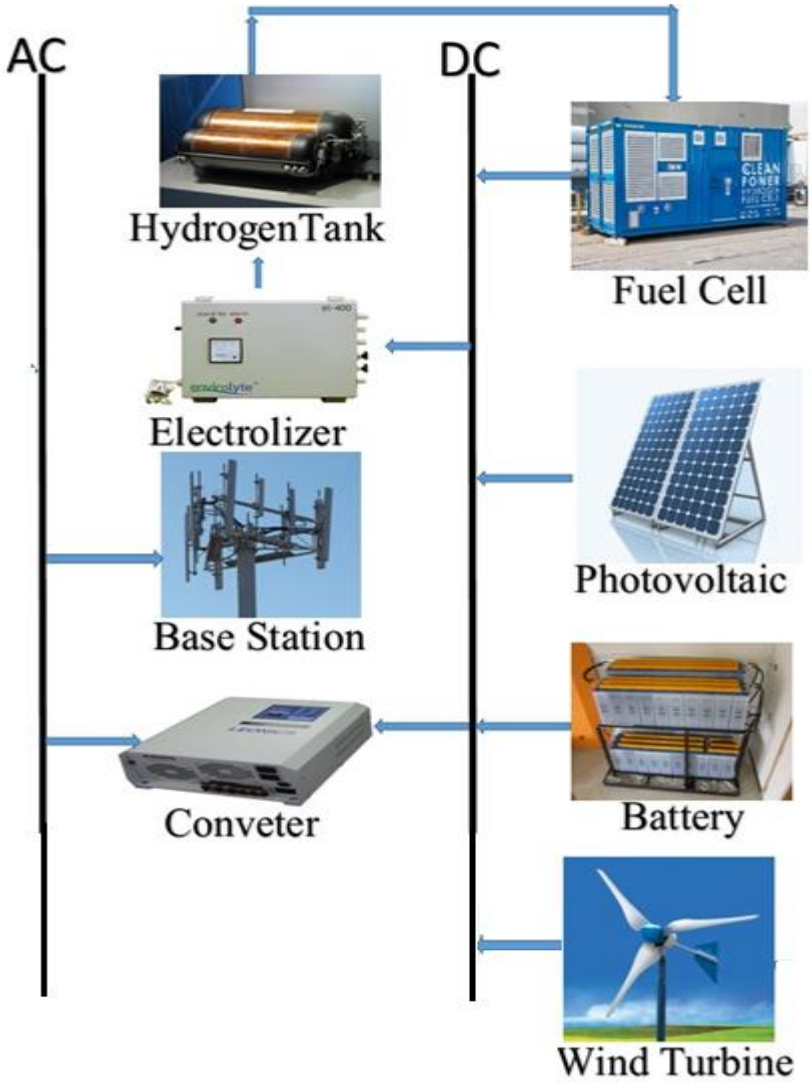

Figure 3. 11. The schematic diagram of the experimental setup.

The RES's and BS of the HRES are controlled by a selected system dispatch strategie. Furthermore, these RES's can share the load demand to prevent the problem of power shortages. The functions of each component of the HRES are presented below:

I. **PV Panels**: These panels are responsible for harvesting and converting the SI into energy.

II. **Wind Turbine**: This turbine works as a secondary power source in the event where the PV panels are not able to meet the load demand.

III. **Fuel Cell**: This FC works as a secondary power source in the event where the PV panels and WT are not able to meet the load demand.

IV. **Battery Storage**: The BS stores the surplus excess energy and supplies the power when the PV, WT and FC are not able to meet the load demand.

V. **Charge Controller**: This controller protects the BS from overvoltage and overcharging by regulating the rate the electric current is used to charge or the amount of current drawn from the BS.

VI. **Bi-Directional Inverter**: This inverter is connected to the Alternating Current (AC) and the Direct Current (DC) bus-bars for converting the AC to DC or DC to AC depending on where the power is needed. Furthermore, the inverter records the daily, monthly or yearly energy production of the system and can help prevent electrical problems.

VII. **Control system**: This acts as the brain of a sophisticated regulation, control, and communication system. In the remote interface, wireless modems or network solutions are the most common communication units.

A high degree of operational flexibility is allowed by this arrangement; this translates to the load demand being fulfilled by one energy source or collaborative energy source configurations among the three sources (PV, WT, and FC).

3.5. Chosen Optimisation Method

As presented in the literature review, numerous methods can be employed for optimisation of an HRES. Simulation programmes are some of the methods that are commonly employed by researchers to perform optimisation and simulation of an HRES [47]. The optimum configuration of the HRES can be obtained by utilising one of these computer optimisation and simulation programmes [47]. These programmes compare the energy production, costs and performance of distinct system configurations [47]. HOMER, HYBRID2, HOGA, and Transient System Simulation Tool (TRNSYS) are the numerous simulation tools utilised for designing HRESs [47].

Among the various software mentioned above, the HOMER has been selected for optimisation and simulation of the proposed HRES in this study. From the literature, it has been found that HOMER is widely used for simulation and optimisation of HRESs. HOMER can do sensitivity analysis, optimisation and simulation of any designed system [58]. Energy balance computations are performed in the simulation process based on the configuration of the proposed system [58]. A list of configurations after the optimisation process are presented and ranked according to their NPC. The replacement costs, installation cost, fuel cost, O&M costs and the real interest of the proposed system are included in the optimisation computations [58]. The varying factors like SI, WS and costs of the fuel are determined by the sensitivity analysis [58]. Thus, the HOMER is capable of evaluating different designs like a grid-connected and a stand-alone power system [58]. Various forms of graphs and tables are presented in the simulation results [58]. These graphs and tables show the performances of the proposed systems compared to the other configurations [58]. This makes it possible for the results to be compared and evaluated according to the objectives stipulated by the designers of the proposed system [58]. HOMER is capable of optimally sizing the components of an HRES [58]. Furthermore, HOMER also does a

comparison between two simple dispatch strategies [58]. HOMER utilises these two dispatch strategies to determine how the system charges the battery bank. The dispatch strategies include the Load Following (LF) and Cycle Charging Strategy (CC) [58]. In this work, the two dispatch strategies will be presented and discussed to show which one was used in this study and why.

3.5.1. Mathematical Models of the Systems Components in HOMER

In HOMER, any part of a micro-power system that converts, delivers, generates, or stores energy is a component [58]. Only ten types of components are modelled in HOMER [58]. This section describes the way some of these components are modelled in HOMER.

a. PV Model

In HOMER the subsequent Equation is used to compute the output PV power [58]:

$$P_{PV} = Y_{PV} \times f_{PV} \times \left(\frac{G_T}{G_{T,STC}}\right) \times \left[1 + \alpha_p\left(T_c - T_{c,STC}\right)\right], \tag{3.3}$$

where

Y_{PV} is the rated capacity of the PV under Standard Test Conditions (STC) in kW, f_{PV} is the PV derating factor, G_T and $G_{T,STC}$ is the incident of SI on the PV array in the current time-step in kW/m^2 and the incident SI at STC in 1 kW/m^2 respectively, T_C and $T_{C,STC}$ is the PV cell temperature of the in the current time-step in ◦C and the PV cell temperature under STC at 25 ◦C and α_p is the temperature coefficient of power in %/◦C. The following expression is used in calculating the temperature of the PV cell [58]:

$$T_c = \frac{T_a + \left(T_{c,NOCT} - T_{a,NOCT}\right) \times \left(\frac{G_T}{G_{T,NOCT}}\right) \times \left[1 - \frac{\eta_{mp,STC}\left(1 - \alpha_p T_{c,STC}\right)}{\tau\alpha}\right]}{1 + \left(T_{c,NOCT} - T_{a,NOCT}\right) \times \left(\frac{G_T}{G_{T,NOCT}}\right) \times \left(\frac{\alpha_p \eta_{mp,STC}}{\tau\alpha}\right)}, \tag{3.4}$$

where

T_a is the AT in ◦C, $T_{a,NOCT}$ and $T_{C,NOCT}$ is the AT at 20 ◦C at which the Nominal Operating Cell Temperature (NOCT) is defined and the NOCT in ◦C respectively, $G_{T,NOCT}$ is the SI at 0.8 kW/m^2 at which the NOCT is defined, τ is the solar transmittance of any cover over the PV array in %, $\eta_{mp,STC}$ is the maximum power point efficiency under STC in %, and α is the PV array solar absorptance in %. The CI (displayed in Figure 5.4) is represented by the Equation below (58):

$$K_T = \frac{H_{ave}}{H_{O,ave}}, \tag{3.5}$$

where

H_{ave} is the average monthly radiation on the horizontal surface of the earth in kWh/m^2/day, and $H_{o,ave}$ is the extraterrestrial horizontal radiation on a horizontal surface at the top of the earth's atmosphere in kWh/m^2/day [58]. While the solar radiation solar intensity at the top of the atmosphere of the earth is given by [58]:

$$G_{on} = G_{sc}\left(1 + 0.33cos\frac{360_n}{365}\right), \tag{3.6}$$

where

n is 1 to 365 days of the year, and

$$G_{sc} = solar\ constant\left[\frac{1.367\ kW}{m^2}\right], \tag{3.7}$$

***b*. WT Model**

HOMER employs a three-step process to compute the WT output power in each time-step [58]. HOMER first determines the WS at the hub height of the WT then determines the amount of power the WT can produce at that WS at standard density [58]. The third and final step is where the actual air density power output

value is adjusted accordingly by HOMER [58]. HOMER employs the power-law Equation to determine the WT WS at the hub height utilising the wind speed data collected at the anemometer height as [58]:

$$u(h) = u(h_{an}) \times \left(\frac{h}{h_{an}}\right)^{\alpha}, \tag{3.8}$$

where

$u(h_{an})$ is the WS at anemometer height in m/s, h is the hub height of selected location, h_{an} is the anemometer height in metres and α is the power-law exponent.

Typically the performance of the WT under conditions of standard temperature and pressure (STP) is specified by the power curves [58]. In HOMER the air density ratio is multiplied by the power value predicted by the power curve to adjust to actual conditions [58]. The subsequent Equation is used by HOMER:

$$P_{WT} = P_{WT,STP} \times \left(\frac{\rho}{\rho_0}\right), \tag{3.9}$$

where

$P_{WT,\ STP}$ is the WT output power at STP in kW, ρ is the actual air density in kg/m^3, P_{WT} is the WT output power in kW, ρ_0 is the air density at STP (1.225 kg/m^3).

c. BS Model

HOMER computes the maximum amount of power that the storage bank can absorb in each time-step [58]. HOMER utilises this maximum charge power to determine how much surplus power should a CC generator produce or whether the entire attainable surplus renewable power can be absorbed by the storage bank [58]. From one time-step to the next, the maximum charge power varies in accordance with its recent charge, discharge history and State of Charge (SOC) [58].

Three separate limitations are imposed by HOMER on the maximum charge power of the storage bank [58]. The first limitation comes from the kinetic storage model [58]. The second limitation relates to the maximum charge rate of the storage component, which is the A/Ah value [58]. The third limitation relates to the storage component's maximum charge current [58]. In the kinetic battery model the maximum amount of power that can be absorbed by the two-tank system is described by the subsequent Equation [58]:

$$P_{bs,cmax,kbm} = \frac{kQ_1e^{-k\Delta t}+Qkc(1-e^{-k\Delta t})}{1-e^{-k\Delta t}+c(k\Delta t-1+e^{-k\Delta t})}, \quad (3.10)$$

where

Δt is the length of the time-step in hours, *k* is the storage rate constant [h-1], *c* is the storage capacity ratio, *Q* is the total amount of energy in kWh in the storage bank at the beginning of the time-step, Q_1 is the available energy in kWh in the storage bank at the beginning of the time-step.

For the second limit the maximum charge rate corresponding to the storage charge power is given by the subsequent Equation:

$$P_{bs,cmax,mcr} = \frac{(1-e^{-k\Delta t})(Q_{max}-Q)}{\Delta t}, \quad (3.11)$$

where

Q_{max} is the total capacity of the storage bank in kWh and *αc* is the storage bank's maximum charge rate at A/Ah.

For the third limit the maximum charge current corresponding to the maximum storage bank charge power is given by the subsequent Equation:

$$P_{bs,cmax,mcc} = \frac{N_{bs}I_{max}V_{nom}}{1000}, \quad (3.12)$$

where

V_{nom} is the storage bank's nominal voltage in volts, I_{max} is the maximum charge current of the BS in amperes, and N_{batt} is the number of batteries in the storage bank.

HOMER sets the least of these three values equal to the maximum storage charge power, with an assumption that each applies after charging losses, hence [58]:

$$P_{bs,cmax,mcc} = \frac{MIN(P_{bs,cmax,kbm} P_{bs,cmax,mcr} P_{bs,cmax,mcc})}{\eta_{batt,c}}, \quad (3.13)$$

where

$\eta_{batt,c}$ is the storage charge efficiency.

***d*. DG Model**

DG's are used as alternative energy sources in cases where there is no access to grid or interruption to electrical energy [58]. DG, which are also preferred as back-up power, provide a robust and reliable energy supply due to their structures [58]. In HOMER the fuel consumption per hour of a diesel-fuelled DG is calculated by using the subsequent Equation [58]:

$$F = F_0 * Y_{gen} + F_1 * P_{gen}, \quad (3.14)$$

where:

P_{gen} is the electrical output of the generator (kW), Y_{gen} is the rated capacity of the generator (kW), F_1 is the fuel curve slope (L/hr/kW), F_o is the fuel curve intercept coefficient (L/hr/kW), and F is the fuel consumption rate (L/hr).

3.5.2. Mathematical Models of the Costs in HOMER

HOMER utalises the total NPC to represent the LCC of a system and as the main economic value to rank all system configurations in the optimisation results [58]. The NPC of a system represents the recent value of all the costs incurred by the system over its life-span, minus the recent value of the entire revenue it accumulates over its life-span [58]. Furthermore, the NPC is the basis from which the COE and the Total Annualised Cost (TAC) are calculated [58]. The TAC is the annualised value of the total NPC. Included in the NPC's are the replacement costs, capital costs, fuel costs, O&M costs, emission penalties, miscellaneous costs such as penalties resulting from pollutant emissions, and the expenses of buying electricity from the grid [58]. In HOMER, the total NPC is calculated by the summation of the total discounted cash flows in each year of the life-span of the project [58]. In HOMER the TAC is determined using the subsequent Equation:

$$TAC = CRF\left(i_{dr}, R_{pjt}\right) * T_{NPC}, \tag{3.15}$$

where

T_{NPC} is the systems total NPCs in ZAR/yr, i_{dr} is the actual discounted rate annually in %, R_{pjt} lifetime of the project in years, and *CRF* is the capital recovery factor obtained by utilising the Equation below [58]:

$$CRF(i, N) = \frac{i(1+i)^N}{(1+i)^N - 1}, \tag{3.16}$$

where

i is the real interest rate annually and *N* is the number of years.

In HOMER the COE is known as the average cost of useful electrical energy per kilowatt-hour produced by the system [58]. HOMER utilises the TAC to

determine the COE [58]. The following Equation is used in HOMER to calculate the COE:

$$COE = \frac{TAC - C_{boiler} + H_{srvd}}{E_{srvd}}, \quad (3.17)$$

where

E_{srvd} is the total electrical load served in kWh/year, H_{srvd} is the total thermal load served in kWh/year and C_{boiler} is the boiler marginal cost in $/kWh.

In HOMER the penalty for GHG emissions is calculated effortlessly utilising the subsequent Equation below [58]:

$$C_{emi} = \frac{CO_{2,C}CO_{2,E} + CO_C CO_E + UHC_C UHC_E + PM_C PM_E + SO_{2,C}SO_{2,E} + NOx_E NOx_C}{1000}, \quad (3.18)$$

where

$CO_{2,E}$ is the annual CO_2 emissions in kg/yr, $CO_{2,C}$ is the cost of CO_2 emissions in $/t, UHC_E is the annual unburned hydrocarbons (UHC) emissions in kg/yr, UHC_C is the cost of UHC emissions in $/t, CO_E is the annual carbon monoxide (CO) emissions in kg/yr, CO_C is the cost of CO emissions in $/t, PM_E is the annual particulate matter (PM) emissions in kg/yr, PM_C is the cost of PM emissions in $/t, $SO_{2,E}$ is the annual sulfur dioxide (SO_2) emissions in kg/yr, $SO_{2,C}$ is the cost of SO2 emissions in $/t, NOx_E is the annual nitrogen oxide (NOx) emissions in kg/yr, and NOx_E is the cost of NOx emissions in $/t.

HOMER applies an „annual real interest rate" rather than a „nominal interest rate" because it assumes that all prices escalate at the same rate [58]. In HOMER salvage costs are also taken into consideration when determining the NPC [58]. These salvage costs are the residual value of the components of the

power system at the end of the project lifetime [58]. The salvage value (SV) is determined by using the subsequent Equation:

$$C_{SV} = C_{rep} * \left(\frac{R_{rem}}{R_{comp}}\right), \quad (3.19)$$

where

R_{comp} is the component lifetime in years, C_{rep} is the replacement cost in $ and R_{rem} is the remaining life of the component at the end of the project lifetime which is computed by using the subsequent Equation:

$$R_{rem} = R_{comp} - (R_{proj} - R_{rep}), \quad (3.20)$$

where

R_{proj} is the project lifetime in years, R_{rep} is the replacement cost duration which is determined by using the subsequent Equation:

$$R_{rep} = R_{comp} * INT\left(\frac{R_{proj}}{R_{comp}}\right), \quad (3.21)$$

where

INT() is a function that returns the integer amount of a real number.

3.5.3. System Model in HOMER

The components that form part of the HOMER simulation of the HRES include PV, WT, FC, electrolyser, hydrogen storage tank, DG, BS, and a bi-directional converter. The DG was included in the HOMER HRES architecture to simulate the base case of the DG/BS system current utilised to power the LTE BTS in remote or rural areas. The BS works as a back-up for instances whereby the PV, WT and FC are not able to meet the load demand. In the system architecture, all the components are coupled with the DC bus-bar except for the

LTE BTS load, and the DG which are coupled to the AC bus-bar as shown in Figure 3.12.

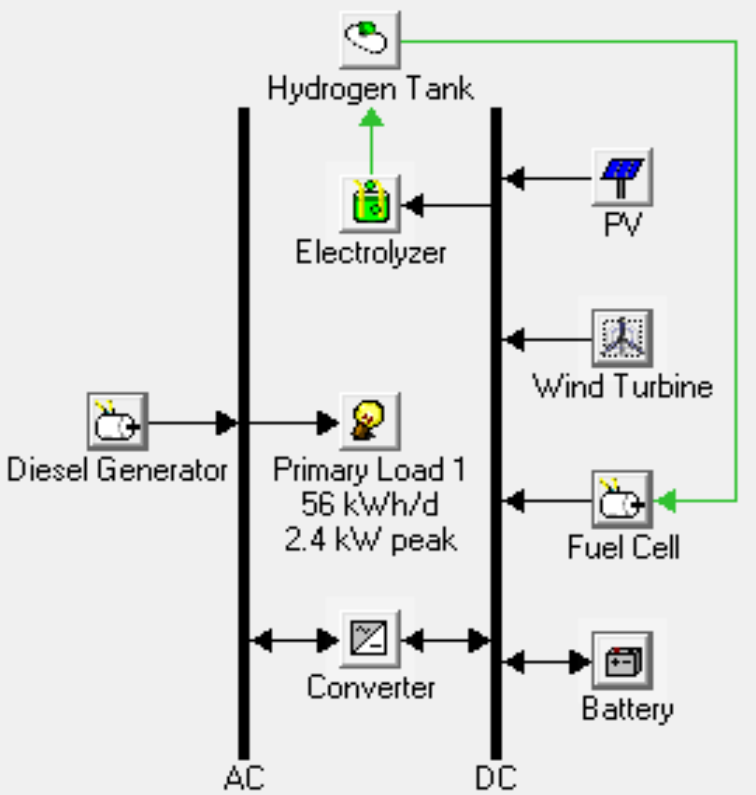

Figure 3. 12. System model for HOMER simulation.

The sizes of the components were selected based upon a couple of restrictions and assumptions. The minimum size of all components within the system was limited to 3 kW. The specifications of the generic components found in HOMER have not been modified in any way. In favour of PV as the primary source of power, the number of WT in the system has been limited to one. Finally, the DG size has been limited to a maximum of 10kW to match its energy production. This was done to favour the use of RES over the use of the DG. The optimal sizes of the components were selected based on gradually modifying the size of the components according to their costs and elimination of DG as a source of power.

3.5.4. Specifications and Costs of the Systems Components

This section details the specifications, HOMER search space capacity or quantity values and the techno-economics of the input parameters of the components used in HOMER for optimisation and simulation of the proposed HRES.

a. Specifications of the Photovoltaic Panels

In this study, the solar panel selected is the Canadian HiKU CS3W-390-405P-400W [59]. This panel is the first poly module exceeding 400 W and has high efficiency. This panel also lessens the installation costs and COE of the system. Figure 3.13 shows the manufacturer's I-V curve profile of the PV between different SI. ANNEXURE A-6 provides the technical specifications of the panel.

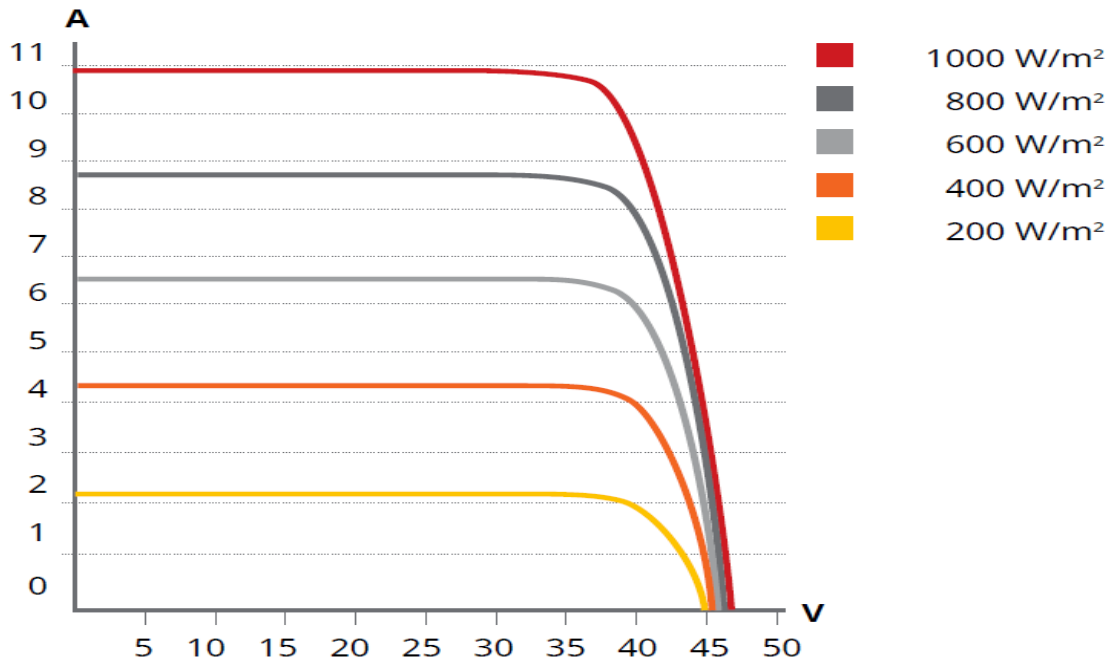

Figure 3. 13. Canadian HiKU CS3W-390-405P-400W Power Profile.

b. Specifications of the Wind Turbine

The chosen WT in this study is the Kestrel e400n 3 kW WT [60]. Kestrel e400n WT's can operate at full capacity in all wind conditions while protecting itself in extreme weather conditions. As a result, it offers superior performance with absolute WT protection. The number of WT's was limited to one in the HOMER search space. ANNEXURE A-7 provides the technical specifications of the WT. The manufacturer's datasheet provided the output of the chosen WT under different WS's. Based on these values the polynomial of the first degree was used to model the Equation that can be used to model the power curve of the WT. This curve shows how the WT behaves under different WSs. The Matrix Laboratory (MATLAB) programme was used to model the trend line Equation using the polynomial of the fourth degree. The obtained polynomial fitting Equation of the WT power curve is shown below:

$$P_{WT} = -1.149v^4 + 24.779v^3 - 129.87v^2 + 249.77v - 85.822 \qquad (3.22)$$

where
P_{WT} is the power produced in kW and v is the WS in m/s.

This Equation was utilised to determine the output power of the WT at different WSs. Figure 3.14 shows the power curve of the chosen WT under different WSs.

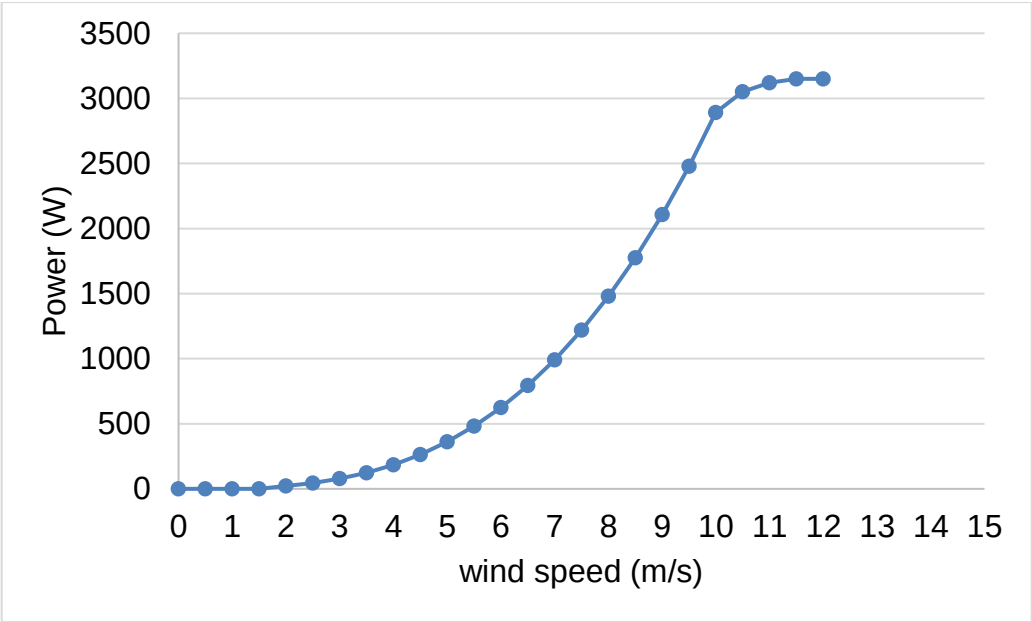

Figure 3. 14. The Kestrel e400n Wind Speed/Power Profile.

c. Specifications of the Fuel Cell

The FC chosen in this study is the Horizon H-3000 PEM Fuel Cell-3000 W [61]. This FC is a self-humidified, air-cooled/air fed hydrogen FC. Because this FC is cooled by air, there is no need for huge, expensive and sophisticated water cooling systems. Additionally, this FC is efficient, semi-integrated, reliable and reduces the use of peripherals which makes it lighter in weight. Figure 3.15 shows the manufacturer's capacity/discharge current profile and the cycles of failure/depth of the discharge profile of the chosen FC. The size of the electrolyser was chosen to be 20 kW and was inputted into the HOMER search space. The size of the hydrogen storage tank was chosen to be 10 kg and was inputted into the HOMER search space. ANNEXURE A-8 provides the technical specifications of the FC. The manufacturer's datasheet provided the fuel consumption of the chosen FC under different outputs. Based on these values the polynomial of the second degree was used to model the Equation that can be used to model the fuel curve of the FC. This curve shows how the FC

behaves under different loads. The MATLAB programme was used to model the trend line Equation using polynomial of the second degree. The obtained polynomial fitting Equation of the FC fuel curve is shown below:

$$FC_c = 0.000002P^2 + 0.0074P + 0.4333 \quad (3.23)$$

where

P is the power produced in kW and FC_c is the fuel consumption in litres.

This Equation was utilised to determine the fuel consumption of the FC at different loads. Figure 3.15 shows the fuel curve of the chosen FC under different loads.

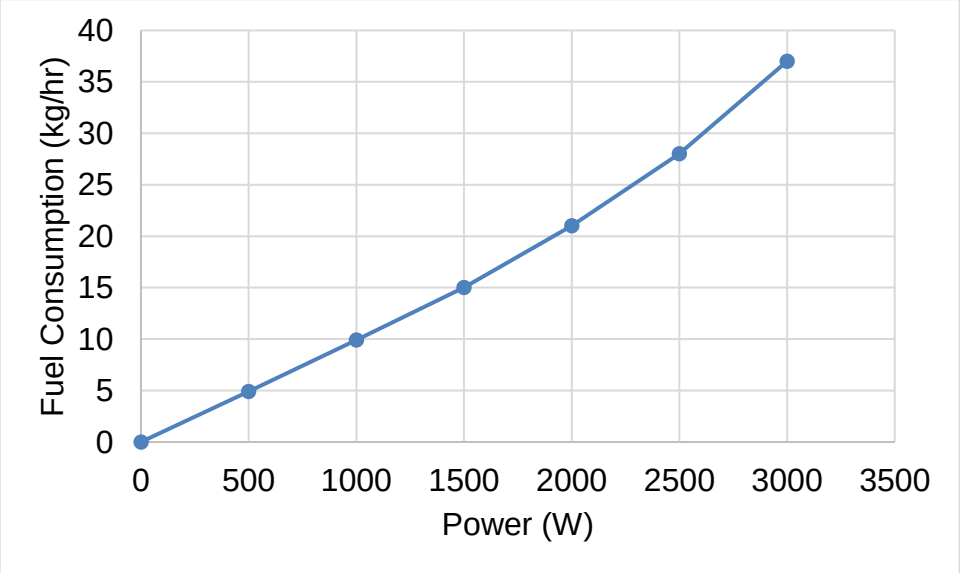

Figure 3. 15. The profile of the Horizon H-3000 PEM FC [45].

d. Specifications of the Battery

The selected battery for this study is a Trojan T-105 (6V-225 Ah) Absorbent Glass Mat (AGM) sealed lead-acid battery [62]. The battery minimum SOC_{min} was set to 40% and the maximum SOC_{max} was set to 100%. Each component's O&M costs are assumed to be 2% of the yearly initial cost. An assumption is made that the replacement of half of the HRES batteries will be done in twenty years. Figure 3.16 shows the manufacturer's capacity/discharge current profile of the chosen battery. ANNEXURE A-9 provides the technical specifications of the battery. The number of batteries was chosen to be 6 and was inputted into the HOMER search space.

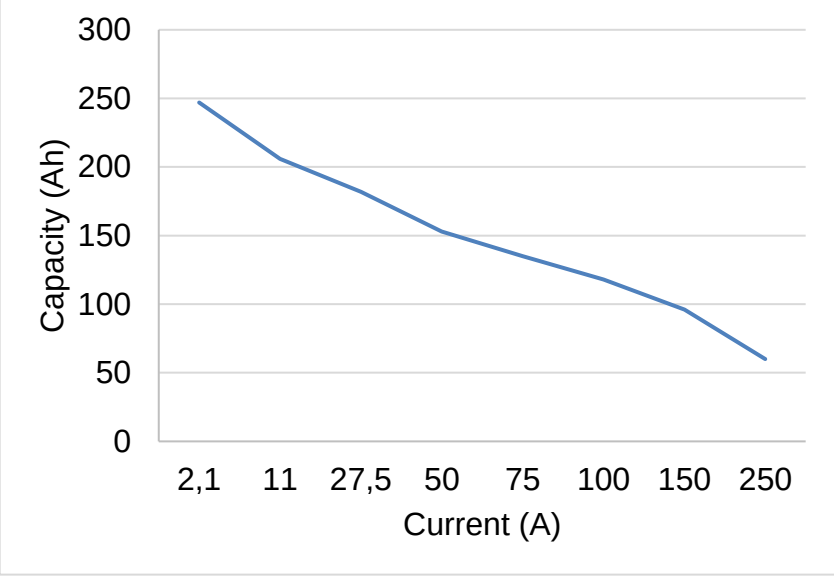

Figure 3. 16. The capacity/discharge current profile of the Trojan T-105 [47].

e. Specifications of the Bi-Directional Inverter

The Bi-Directional Inverter chosen in this study is the Solax X3-hybrid10 10 kW [63]. This Bi-Directional Inverter is highly efficient and intelligent. ANNEXURE A-10 provides the technical specifications of the inverter. The size of the converter was chosen to be 10 kW and was inputted into the HOMER search space.

f. Specifications of the Diesel Generator

The DG chosen in this study is the generic 10 kW fixed capacity DG [58]. The DG size has been limited to a maximum of 10kW to match its energy production. This was done to favour the use of RES over the use of the DG. ANNEXURE A-11 provides the technical specifications of the DG. The manufacturer's datasheet provided the fuel consumption of the chosen DG under three different loads of 50%, 75% and 100%. Based on these values the polynomial of the first degree was used to model the Equation that can be used to model the fuel curve of the DG. This curve shows how the DG behaves under different loads. The MATLAB programme was used to model the trend line Equation using the polynomial of the first degree. The obtained polynomial fitting Equation of the DG fuel curve is shown below:

$$FC_{DG} = 0.436 * P + 0.49, \tag{3.24}$$

where

P is the power produced in kW and F_c is the fuel consumption in litres.

This Equation was utilised to determine the fuel consumption of the DG at different loads. Figure 3.17 shows the fuel curve of the chosen DG under different loads.

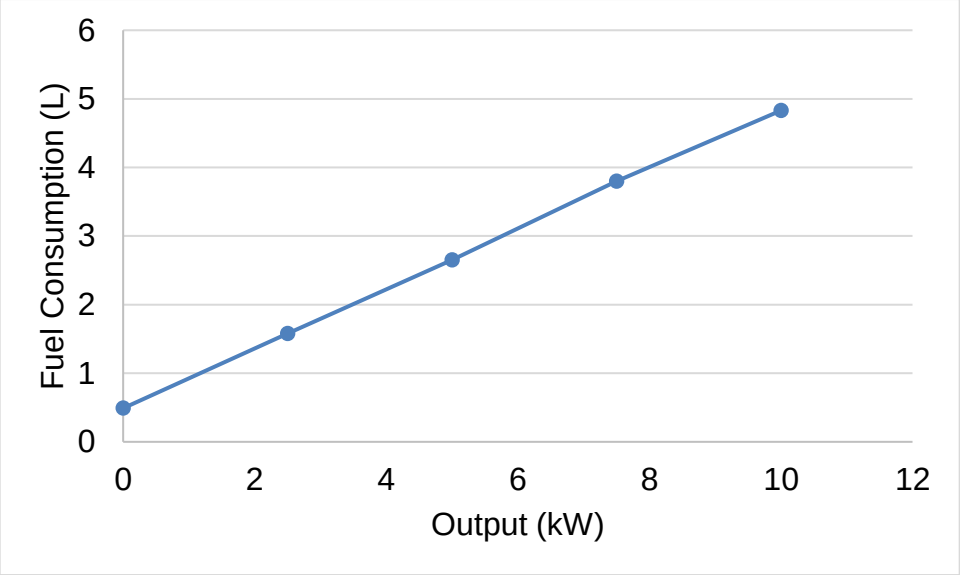

Figure 3. 17. The efficiency curve of the generic 10 kW fixed capacity DG [47].

g. HOMER Search Space Capacity or Quantity Values

The capacity or quantity values of the various components are defined and inputted into the HOMER search space [58]. The values inputted in these search space are used by HOMER for simulating all the systems feasible configurations [58]. Furthermore, these values are used by HOMER to determine the configuration that is optimally efficient [58]. These search space values can be inputted on the component pages as the system is being built [58]. The HOMER search space capacity or quantity values of the various components used in this study are presented below:

The sizes of the PV system computed into the HOMER search space were 10 kW, 20 kW, 30 kW, and 40 kW.

The quantity of the WT computed into the HOMER search space was 1.

The size of the FC computed into the HOMER search space was 3 kW.

The size of the DG computed into the HOMER search space was 10 kW.

The number of BS strings computed into the HOMER search space was 4, 6, 8, 10, 12, 14, 16 and 18.

The sizes of the converter computed into the HOMER search space were 5 kW, 10 kW, 15 kW, and 20 kW.

The sizes of the electrolyser computed into the HOMER search space were 5 kW, 10 kW, 15 kW, and 20 kW.

The sizes of the hydrogen storage tank computed into the HOMER search space were 5 kg, 10 kg, 15 kg, and 20 kg.

These values were used by HOMER to simulate all the feasible configurations in the system and determine the optimally sized configuration.

h. Techno-economics of the Input Parameters of the Components

Table 3.5-3.6 show the techno-economic of the input parameters of the hybrid system components used in HOMER.

Table 3. 5. Techno-economics of the various components [54].

Component	Description	Specification
PV System	Capital cost	R6 450.00/kW
	Cost of replacement	R142.01/kW/year
	O&M cost	R129.00/kW
	Lifetime	25 years
Wind Turbine	Capital cost	R46 500.00/kW
	Cost of replacement	R28 235.00/kW
	Operating and maintenance cost	R930.00/kW
	Lifetime	25 years
Battery	Capital cost	R8 464.58/battery
	Replacement cost	R142.01/year
	O&M cost	R169.28/battery
	Lifetime	20 years
Converter	Capital cost	R11 339.33/kW
	Replacement cost	R8 504.50/kW
	O&M cost	R70.88/kW/year
	Lifetime	20 years

Table 3. 6. Techno-economics of the various components [54].

Component	Description	Specification
Fuel Cell	Capital cost	R42 531.90/kW
	Replacement cost	R35 443.25/kW
	O&M cost	R0.284/hour
	Lifetime	40000 hours
Hydrogen Tank	Capital cost	R15 595.23/kg
	Replacement cost	R13 468.60/kg
	O&M cost	R312.00/year
	Lifetime	20 years
Electrolyser	Capital cost	R21 266.16/kW
	Replacement cost	R17 012.93/kW
	O&M cost	R425.55/kW
	Lifetime	20 years
Diesel Generator	Capital cost	R8500.00/kW
	Replacement cost	R8000.00/kW
	O&M cost	R8.00/hour
	Diesel Price	R14.85/litre
	Lifetime	20 years

3.5.5. Objective Function

The objective function in this study is the minimisation of the total NPC since HOMER utilises the total NPC as the objective function to determine the least costly and optimally sized system [58]. Furthermore, the NPC is used to evaluate the operating features of the HRES [58]. A list of multiple configurations is displayed and ranked by the HOMER according to the NPC of each configuration [58].

3.5.6. Capacity Shortage of the System

In HOMER the shortfall that occurs between the actual amount of operating capacity a system can supply and the required operating capacity is referred to as the capacity shortage [58]. HOMER monitors the system for such shortages and computes the overall amount that occurs throughout the year [58]. The total annual capacity shortage that occurs throughout the year is used to determine the Capacity Shortage Fraction (CSF) at the end of the year [58]. HOMER utilises the CSF to consider a system feasible or not feasible [58]. A system is only considered feasible if the CSF is equal or less than the maximum annual capacity shortage [58]. In HOMER the CSF is determined using the subsequent Equation:

$$CSF = \frac{E_s}{E_{dmd}}, \tag{3.25}$$

where

E_{cs} is the total annual capacity shortage in kWh/year and E_{dmd} is the total electrical demand (primary and deferrable load) in kWh/year.

In this study, the CSF is part of the constraints that the proposed system must meet in order to be considered feasible by HOMER.

3.5.7. Renewable Fraction of the System

HOMER monitors the total annual amount of electrical energy produced by the renewable components of a power system [58]. This is the total electrical energy produced by the RESs of any HRES [58]. HOMER utilises the total electrical energy produced by the RES's to compute the RF [58]. The RF ranges between 0 and 1 and shows the fraction of energy supplied to the load that comes from RES's [58]. In HOMER the RF is determined using the subsequent Equation:

$$RF = \frac{E_{nren}+H_{nren}}{E_{srvd}+H_{srvd}}, \quad (3.26)$$

where:

H_{srvd} is the total thermal load served in kWh/year, E_{srvd} is the total electrical load served in kWh/year, H_{nren} is the non-renewable thermal production in kWh/year, $E_{grid,sales}$ is the energy sold to the grid in kWh/year (included in E_{served}), and E_{nren} is the non-renewable electrical production in kWh/year.

In this study, the RF is part of the constraints that the proposed system must meet in order to be considered feasible by HOMER.

3.5.8. Constraints

For the proposed system to be concluded feasible, several constraints have to be met [58]. HOMER utilises the minimum RF, maximum annual CSF, operating reserve as a percentage of annual peak load, operating reserve as a percentage of hourly load, operating reserve as a percentage of WT power output, and operating reserve as a percentage of PV power output as the constraints that a system has to meet in order to be considered feasible or infeasible [58]. Systems that do not satisfy the specified constraints are discarded by HOMER [58]. The discarded systems do not appear in the optimisation or sensitivity results [58]. The constraints that were inputted into the HOMER constraints space and utilised to determine whether the proposed system is feasible or infeasible are presented in Table 3.7.

As seen in Table 3.5, 10% of the hourly load was set as an operating reserve to allow for no capacity shortage. Furthermore, the operating reserve of the PV and WT output power was set at 25% and 50%. The operating reserve ensures the reliability of the electricity supply because it serves a surplus operating capacity

and as a safe limit [58]. This in-turn assists the system to meet the sudden decrease or increase in load supply in-spite of the fluctuations of the PV and WT power supply [58]. These constraints data in Table 3.7 were computed into the HOMER.

Table 3. 7. Simulation Constraints.

Minimum RF	0%
Maximum annual CSF	0%
Operating reserve as a percentage of annual peak load	0%
Operating reserve as a percentage of hourly load	10%
Operating reserve as a percentage of WT power output	50%
Operating reserve as a percentage of PV power output	25%

3.5.9. System Control in HOMER

In HOMER the controller component lets the user dictate how a system operates during the simulation process [58]. This controller utilises a unique dispatch strategy or control algorithm to dictate how the HOMER engine operates the DGs and the BS to meet the load [58]. By default, HOMER utilises two system dispatch strategies to control the operation of the DGs and the BS of any system [58]. These two dispatch strategies are the LF dispatch strategy and the CC dispatch strategy [58]. These two dispatch strategies are a set of rules that govern the operation of the DG and the BS in instances where there isn't adequate RE to supply the load [58]. To find the optimal strategy between these

two dispatch strategies many factors are considered [58]. These factors include the sizes of the DGs and BS, the character of the RERs, the amount of renewable power in the system, the O&M cost of the DGs, and the price of fuel [58]. HOMER allows the user to choose both the dispatch strategies for simulation [58]. In the case where both these strategies are chosen for simulation, each system will be simulated using both dispatch strategies to show which is the optimal best amongst the two [58].

In this study, the LF strategy was chosen in the optimisation and simulation of the proposed HRES. This LF strategy allows for the DG to only produce enough power to meet the demand the moment it is needed [58]. The serving of the deferrable load or charging of the BS bank is done by the RESs [58]. This strategy is optimal in systems that have a significant amount of renewable power that sometimes surpasses the load demand [58].

3.6. Description of the Proposed Method

The main stages that properly explain the proposed methodology are presented below:

The meteorological data, component specifications, load profile, and constraints are fed into HOMER for the simulation process. From then on, simulation of each and every feasible arrangement in the search space is going to be done in every single time-step of the year, and the sought after results such as NPC, RF, and CSF will be computed for additional utilisation.

CHAPTER FOUR: RESULTS AND DISCUSSION

This chapter presents the HOMER optimisation results for all selected sites for the proposed HRES. The HOMER performed three main procedures, namely; optimisation, classical analysis simulation, and sensitivity analysis. The behaviour of each system configuration over a lengthy period in a given setting was determined by the simulation process. The purpose of this process was to determine the optimally sized and feasible system that can meet the load demands of the LTE BTS load. The NPC is the one used in HOMER to determine the optimally designed and least costly system amongst the feasible configurations. The proposed HRES will be considered as an optimal remedy for the chosen LTE BTS site if the load demands of the LTE BTS are met at minimum NPC, zero GHG emissions, zero system capacity shortage and 100% RF.

The simulation results are dealt with analytically in this section. All the simulation results from all sites considered in this study are presented, which are tracked by the outcomes of the NPC. Also, an emissions analysis is performed for the consideration of the environmental aspect of the configuration of the system. The proposed PV/WT/FC/BS HRES is compared to the current DG/BS only system used to power LTE BTS in rural areas. The two systems are analysed to show the superiority of the proposed HRES over the DG/BS only system.

4.1. Cost Optimisation Results

The HOMER software revealed that 36826 feasible solutions were simulated after the parameters were computed into the configuration of the system. The NPC for different systems were simulated in HOMER and evaluated for comparison analysis. The HOMER simulation results for all the sites considered in this study are presented in Figure 4.1 to 4.6. All feasible configurations were

ranked according to their NPC from lowest to highest as demonstrated in Figure 4.1 to 4.6. The HOMER cost optimisation results for all sites are also presented in a tabular and graphical form in Table 4.1 and Figure 4.7.

Architecture											Cost	System
									PV System (kW)	Wind Turbine	Fuel Cell (kW)	Diesel Generator (kW)	Battery Storage	NPC (R)	Ren Frac (%)
									30,0	1	3,00		16	R976 118	100
									20,0			10,0		R1,53M	30,7
									20,0	1		10,0		R1,60M	32,7
										1		10,0	4	R1,61M	25,4
												10,0	4	R2,03M	0
												10,0		R2,04M	0
										1		10,0		R2,14M	0

Figure 4. 1. HOMER optimisation results for Mafikeng.

Architecture											Cost	System
									PV System (kW)	Wind Turbine	Fuel Cell (kW)	Diesel Generator (kW)	Battery Storage	NPC (R)	Ren Frac (%)
									40,0	1	3,00		12	R1,24M	100
									20,0			10,0		R1,54M	30,2
									20,0	1		10,0		R1,62M	31,7
										1		10,0	4	R1,75M	17,7
												10,0	4	R2,03M	0
												10,0		R2,04M	0
										1		10,0		R2,14M	0

Figure 4. 2. HOMER optimisation results for Rustenburg.

Architecture											Cost	System
									PV System (kW)	Wind Turbine	Fuel Cell (kW)	Diesel Generator (kW)	Battery Storage	NPC (R)	Ren Frac (%)
									40,0	1	3,00		12	R1,24M	100
									20,0			10,0		R1,54M	30,1
									20,0	1		10,0		R1,62M	31,7
										1		10,0	4	R1,73M	18,5
												10,0	4	R2,03M	0
												10,0		R2,04M	0
										1		10,0		R2,14M	0

Figure 4. 3. HOMER optimisation results for Potchefstroom.

Architecture											Cost	System
									PV System (kW)	Wind Turbine	Fuel Cell (kW)	Diesel Generator (kW)	Battery Storage	NPC (R)	Ren Frac (%)
									30,0	1	3,00		16	R969 323	100
										1		10,0	4	R1,50M	31,6
									20,0			10,0		R1,53M	31,0
									20,0	1		10,0		R1,59M	33,5
												10,0	4	R2,03M	0
												10,0		R2,04M	0
										1		10,0		R2,13M	0

Figure 4. 4. HOMER optimisation results for Vryburg.

Architecture												Cost	System
									PV System (kW)	Wind Turbine	Fuel Cell (kW)	Diesel Generator (kW)	Battery Storage	NPC (R)	Ren Frac (%)
									40,0	1	3,00		16	R1,06M	100
									20,0			10,0		R1,54M	30,4
									20,0	1		10,0		R1,61M	32,3
										1		10,0	4	R1,64M	23,6
												10,0	4	R2,03M	0
												10,0		R2,04M	0
										1		10,0		R2,14M	0

Figure 4. 5. HOMER optimisation results for Lichtenburg.

Architecture												Cost	System
									PV System (kW)	Wind Turbine	Fuel Cell (kW)	Diesel Generator (kW)	Battery Storage	NPC (R)	Ren Frac (%)
									40,0	1	3,00		16	R1,06M	100
									20,0			10,0		R1,54M	30,3
									20,0	1		10,0		R1,61M	32,1
										1		10,0	4	R1,64M	23,6
												10,0	4	R2,03M	0
												10,0		R2,04M	0
										1		10,0		R2,14M	0

Figure 4. 6. HOMER optimisation results for Klerksdorp.

Table 4. 1. HOMER optimisation results according to NPC.

Configuration	Total NPC					
	Site 1	Site 2	Site 3	Site 4	Site 5	Site 6
PV/WT/FC/BS	R976 118.00	R1 240 000.00	R1 240 000.00	R969 323.00	R1 060 000.00	R1 060 000.00
PV/DG	R1 530 000.00	R1 540 000.00	R1 540 000.00	R1 530 000.00	R1 540 000.00	R1 540 000.00
PV/WT/DG	R1 600 000.00	R1 620 000.00	R1 620 000.00	R1 590 000.00	R1 610 000.00	R1 610 000.00
WT/DG/BS	R1 610 000.00	R1 750 000.00	R1 730 000.00	R1 500 000.00	R1 640 000.00	R1 640 000.00
DG/BS	R2 030 000.00	R2 030 000.00	R2 030 000.00	R2 030 000.00	R2 030 000.00	R2 030 000.00
DG	R2 040 000.00	R2 040 000.00	R2 040 000.00	R2 040 000.00	R2 040 000.00	R2 040 000.00
WT/DG	R2 140 000.00	R2 140 000.00	R2 140 000.00	R2 130 000.00	R2 140 000.00	R2 140 000.00

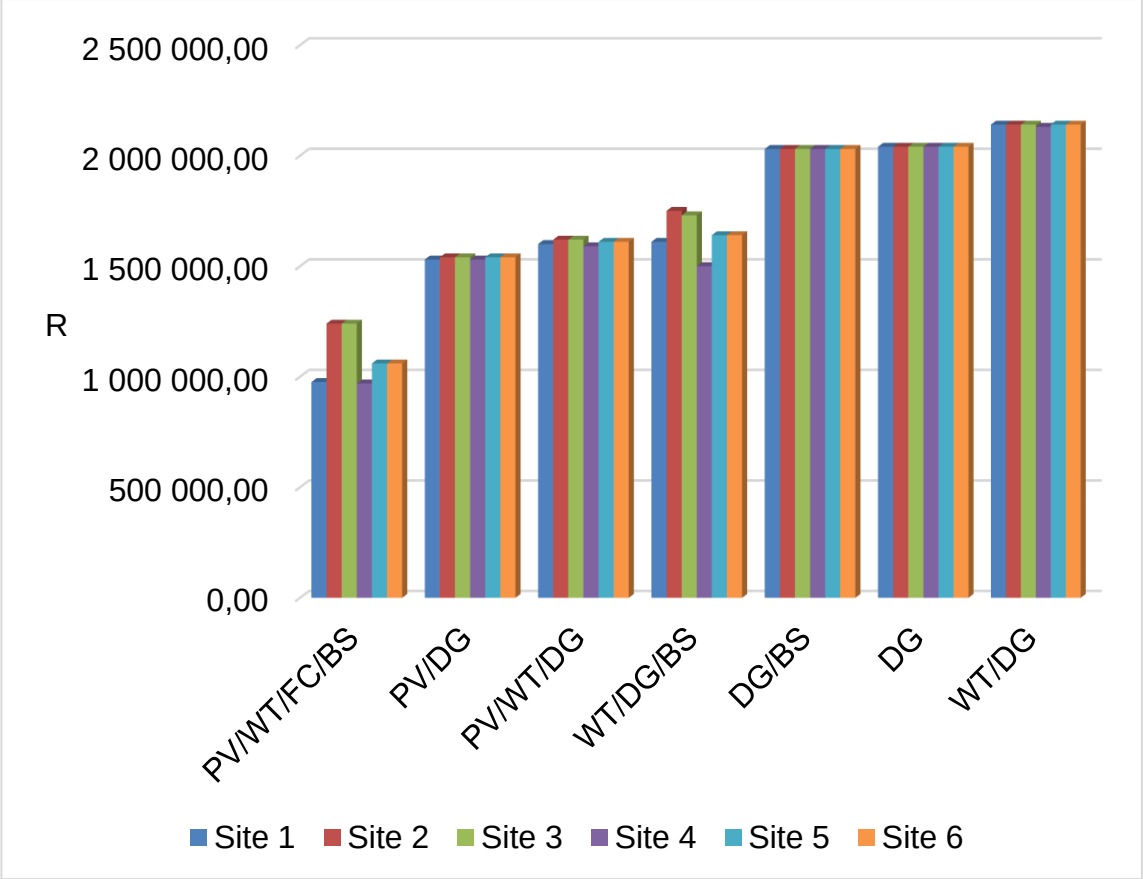

Figure 4. 7. HOMER optimisation results according to NPC.

As can be seen from Table 4.1 and Figure 4.1 the proposed HRES has the least NPC in comparison to the other configurations. These results show that in all sites, the proposed HRES is the least costly system. This shows that the proposed HRES has met one of the objectives of the study and is considered as the most optimally sized HRES for powering the LTE BTS in all locations in this study. Furthermore, the maximum NPC for the proposed HRES is R1 240 000.00 and the maximum NPC for the DG/BS system is R2 030 000.00, respectively. These figures clearly show that the proposed HRES when compared to the DG/BS system, has reduced the NPC by as much as 64%.

4.2. GHG Emissions Results

The HOMER CO_2 emissions results for all sites are presented in Table 4.2 and Figure 4.8.

Table 4. 2. HOMER CO_2 emission results for all sites.

Configuration	Total CO_2					
	Site 1	Site 2	Site 3	Site 4	Site 5	Site 6
PV/WT/FC/BS	0	0	0	0	0	0
PV/DG	17679	17804	17832	17620	17770	17798
PV/WT/DG	17183	17436	17442	16974	17274	17324
WT/DG/BS	19034	21001	20792	17442	19484	19484
DG/BS	26490	26490	26490	26490	26490	26490
DG	27370	27370	27370	27370	27370	27370
WT/DG	27281	27311	27307	27146	27297	27297

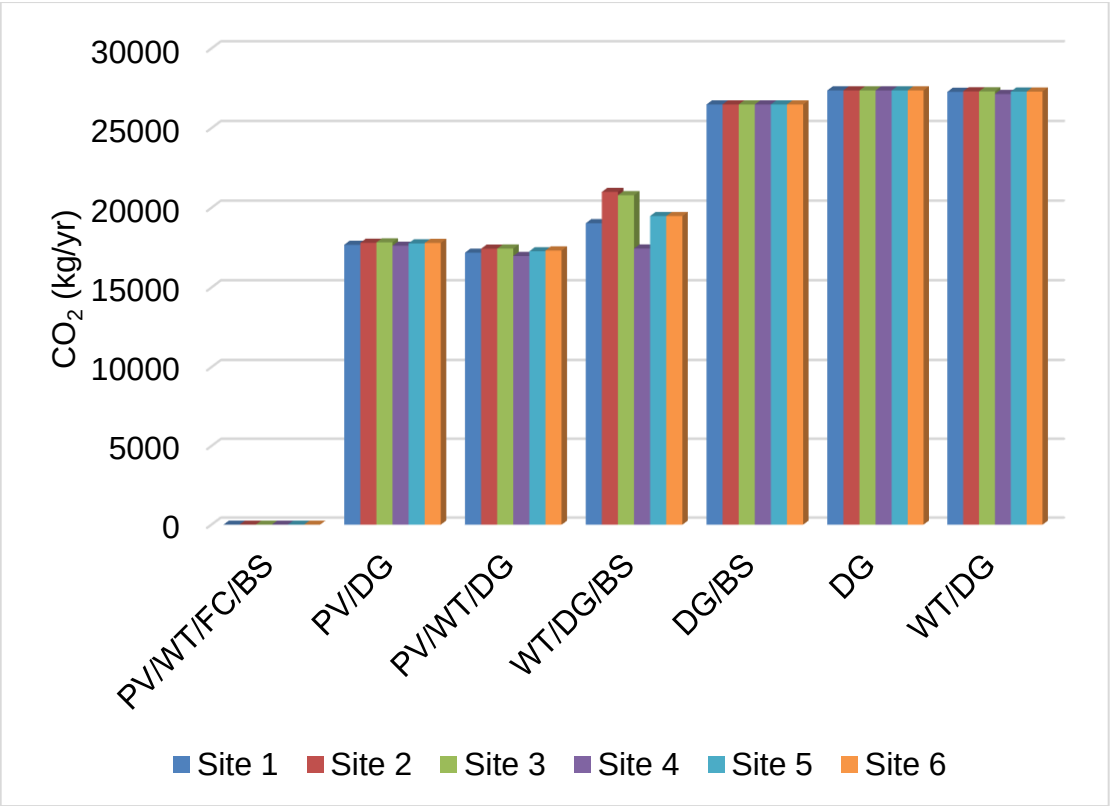

Figure 4. 8. CO_2 emissions for all sites.

As can be seen from Table 4.2 and Figure 4.8 the proposed HRES has zero CO_2 emissions in comparison to the other configurations. These results show that in all sites, the proposed HRES is the most environmentally-friendly system. This shows that the proposed HRES has met one of the objectives of the study and is considered as the most environmentally-friendly HRES for powering the LTE BTS in all locations in this study. Furthermore, the proposed HRES produced zero emissions in comparison to the DG/BS system that produced 27370 kg of carbon dioxide per year in all sites. This shows that the proposed HRES has reduced the GHG emissions by as much as 100% as it did not produce any of the GHG emissions that were produced by the DG/BS system. These results show that in all sites, the proposed HRES has eliminated the emission of GHG's when compared to the conventional DG/BS system.

4.3. Renewable Fraction Results

The HOMER RF results for all sites are presented in Table 4.3 and Figure 4.9.

Table 4. 3. HOMER RF results for all sites.

Configuration	Total RF					
	Site 1	Site 2	Site 3	Site 4	Site 5	Site 6
PV/WT/FC/BS	100	100	100	100	100	100
PV/DG	30.7	30.2	30.1	31	30.4	30.3
PV/WT/DG	32.7	31.7	31.7	33.5	32.3	32.1
WT/DG/BS	25.4	17.7	18.5	31.6	23.6	23.6
DG/BS	0	0	0	0	0	0
DG	0	0	0	0	0	0
WT/DG	0	0	0	0	0	0

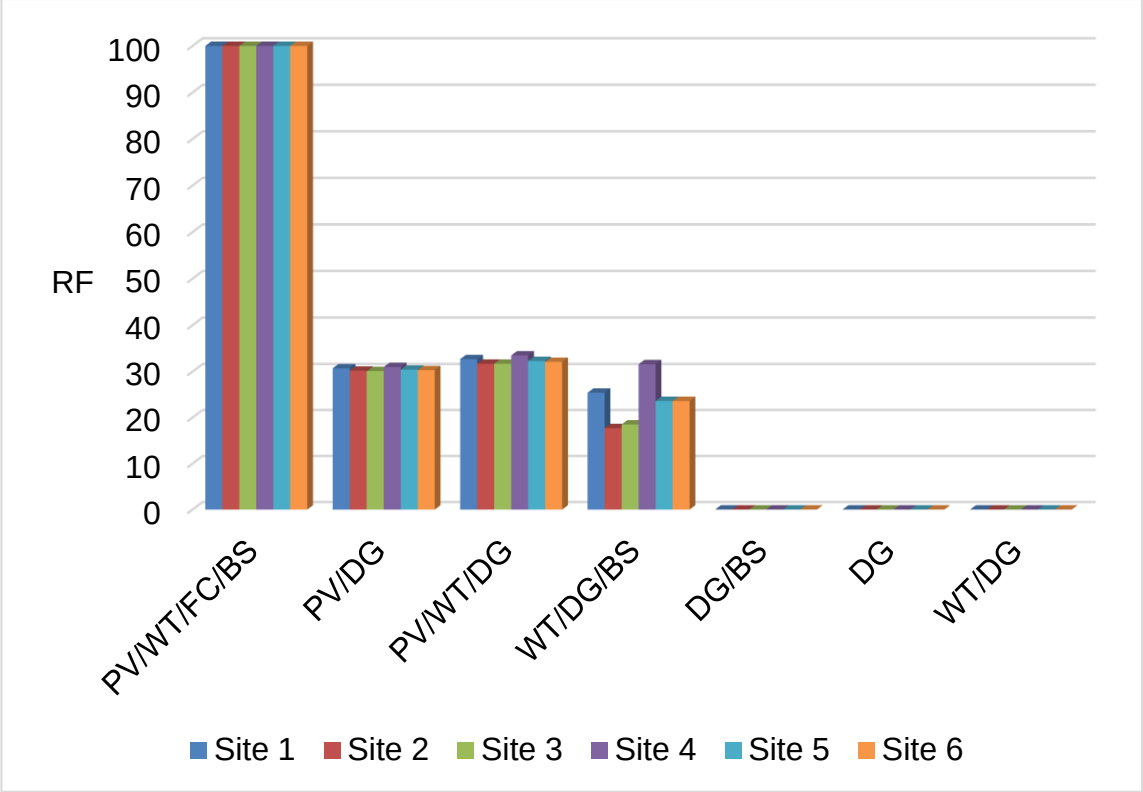

Figure 4. 9. HOMER RF results for all sites.

As can be seen from Table 4.3 and Figure 4.9 the proposed HRES has the highest RF in comparison to the other configurations. These results show that in all sites, the energy produced by the proposed HRES comes from only RES's which makes it the most environmentally-friendly system. This shows that the proposed HRES has met one of the objectives of the study and is considered as the most environmentally-friendly HRES for powering the LTE BTS in all locations in this study. Furthermore, the proposed HRES has RF of one in comparison to the DG/BS system that has zero RF in all sites. This shows that the proposed HRES has increased the RF by as much as 100% as it produced all its energy only from RESs. These results show that in all sites, the proposed HRES has eliminated the need for DG as a source of power for LTE BTS in rural areas.

4.4. Capacity Shortage Results

The HOMER system capacity shortage results for all sites are presented in Table 4.4 and Figure 4.10.

Table 4. 4. HOMER system capacity shortage results for all sites.

Configuration	Total capacity shortage (kWh/year)					
	Site 1	Site 2	Site 3	Site 4	Site 5	Site 6
PV/WT/FC/BS	0	0	0	0	0	0
PV/DG	0	0	0	0	0	0
PV/WT/DG	0	0	0	0	0	0
WT/DG/BS	6.32	6.99	8.84	8.35	7.49	7.49
DG/BS	13.00	13.00	13.00	13.00	13.00	13.00
DG	13.40	13.40	13.40	13.40	13.40	13.40
WT/DG	9.37	9.80	9.30	11.60	8.91	8.91

Figure 4. 10. HOMER system capacity shortage results for all sites.

As can be seen from Table 4.4 and Figure 4.10 the proposed HRES, the PV/DG system and the PV/WT/DG HRES have zero capacity shortage throughout out the year in comparison to the other configurations. These results show that in all sites, the proposed HRES has zero system capacity shortage which makes it a reliable and efficient system. This shows that the proposed HRES has met one of the objectives of the study which is having a zero capacity shortage and is considered as the most reliable and efficient HRES for powering the LTE BTS in all locations in this study. Furthermore, the proposed HRES has zero system capacity shortage in comparison to the DG/BS system that has a 13 kWh/year capacity shortage in all sites. This shows that the proposed HRES has decreased the system capacity shortage by as much as 100% as it met all the energy demands of the load throughout the year. These results show that in all sites, the proposed HRES has eliminated the capacity shortages that come with using DG/BS system as a source of power for LTE BTS in rural areas.

4.5. Power Flow and Battery State of Charge of the Proposed System

In this section, the details of the 24 h power flow and the battery status of the system are shown and discussed in order to have a better understanding of the operation of the proposed system. The month of June was selected for all the sites considered in this study. The battery status and energy flow for each site are described in detail below:

Site 1: The power flow and the battery SOC of the proposed HRES are shown in Figure 4.11 for the first site. From the Figure, it can be seen that at (00:00–05:00) the BS and the WT were the only ones supplying the load since the PV and FC were not producing any power. From (05:00–06:00) the BS reached its minimum SOC, and the FC was the one supplying the load since the PV and WT were not producing any power. The FC stopped producing power by 07:00. The PV system started to produce power at 06:00. The power produced by the PV system was not enough to meet the load demand, so the WT and the FC assisted the PV to charge the BS and meet the load demand until 07:00. At 07:00 the PV started to produce enough power to meet the load demand and at the same time supply surplus power to the BS for charging. The BS reached its maximum SOC by 17:00. The PV and the WT produced enough power to meet the load demand and charge the BS for the period between 07:00 and 17:00. The PV and the WT worked hand-in-hand from 07:00 to 17:00. The PV stopped producing power by 17:00, and the BS and the WT worked hand-in-hand to meet the load demand for the rest of the day.

Site 2: The power flow and the battery SOC of the proposed HRES are shown in Figure 4.12 for the second site. From the Figure, it can be seen that at (00:00–04:00) the BS was the only one supplying the load since the PV, WT and FC were not producing any power. From (04:00–06:00) the BS reached its minimum

SOC, and the FC was the one supplying the load since the PV and WT were not producing any power. The FC stopped producing power by 07:00. The PV system started to produce power at 06:00. The power produced by the PV system was not enough to meet the load demand, so the WT and the FC assisted the PV to charge the BS and meet the load demand until 07:00. At 07:00 the PV started to produce enough power to meet the load demand and at the same time supply surplus power to the BS for charging. The BS reached its maximum SOC by 16:00. The PV and the WT produced enough power to meet the load demand and charge the BS for the period between 07:00 and 16:00. The PV and the WT worked hand-in-hand from 07:00 to 16:00. The PV stopped producing power by 17:00, and the BS and the WT worked hand-in-hand to meet the load demand for the rest of the day.

Site 3: The power flow and the battery SOC of the proposed HRES are shown in Figure 4.13 for the third site. From the Figure, it can be seen that at (00:00–04:00) the BS was the only one supplying the load since the PV, WT and FC were not producing any power. From (04:00–06:00) the BS reached its minimum SOC, and the FC was the one supplying the load since the PV and WT were not producing any power. The FC stopped producing power by 07:00. The PV system started to produce power at 06:00. The power produced by the PV system was not enough to meet the load demand, so the WT and the FC assisted the PV to charge the BS and meet the load demand until 07:00. At 07:00 the PV started to produce enough power to meet the load demand and at the same time supply surplus power to the BS for charging. The BS reached its maximum SOC by 16:00. The PV and the WT produced enough power to meet the load demand and charge the BS for the period between 07:00 and 16:00. The PV and the WT worked hand-in-hand from 07:00 to 16:00. The PV stopped producing power by 17:00, and the BS and the WT worked hand-in-hand to meet the load demand for the rest of the day.

Site 4: The power flow and the battery SOC of the proposed HRES are shown in Figure 4.14 for the fourth site. From the Figure, it can be seen that at (00:00–06:00) the BS and the WT were the only ones supplying the load since the PV, and FC was not producing any power. The PV system started to produce power at 06:00. The power produced by the PV system was not enough to meet the load demand, so the WT assisted the PV to charge the BS and meet the load demand from (06:00–07:00). At 07:00 the PV started to produce enough power to meet the load demand and at the same time supply surplus power to the BS for charging. The BS reached its maximum SOC by 17:00. The PV and the WT produced enough power to meet the load demand and charge the BS for the period between 06:00 and 18:00. The PV and the WT worked hand-in-hand from 06:00 to 18:00. The PV stopped producing power by 18:00, and the BS and the WT worked hand-in-hand to meet the load demand for the rest of the day.

Site 5: The power flow and the battery SOC of the proposed HRES are shown in Figure 4.15 for the fifth site. From the Figure, it can be seen that at (00:00–04:00) the BS was the only one supplying the load since the PV, WT and FC were not producing any power. From (04:00–06:00) the BS reached its minimum SOC, and the FC was the one supplying the load since the PV and WT were not producing any power. The FC stopped producing power by 07:00. The PV system started to produce power at 06:00. The power produced by the PV system was not enough to meet the load demand, so the WT and the FC assisted the PV to charge the BS and meet the load demand until 07:00. At 07:00 the PV started to produce enough power to meet the load demand and at the same time supply surplus power to the BS for charging. The BS reached its maximum SOC by 16:00. The PV and the WT produced enough power to meet the load demand and charge the BS for the period between 07:00 and 16:00. The PV and the WT worked hand-in-hand from 07:00 to 16:00. The PV stopped producing power by 17:00, and the BS and the WT worked hand-in-hand to meet the load demand for the rest of the day.

Site 6: The power flow and the battery SOC of the proposed HRES are shown in Figure 4.16 for the sixth site. From the Figure, it can be seen that at (00:00–04:00) the BS was the only one supplying the load since the PV, WT and FC were not producing any power. From (04:00–06:00) the BS reached its minimum SOC, and the FC was the one supplying the load since the PV and WT were not producing any power. The FC stopped producing power by 07:00. The PV system started to produce power at 06:00. The power produced by the PV system was not enough to meet the load demand, so the WT and the FC assisted the PV to charge the BS and meet the load demand until 07:00. At 07:00 the PV started to produce enough power to meet the load demand and at the same time supply surplus power to the BS for charging. The BS reached its maximum SOC by 16:00. The PV and the WT produced enough power to meet the load demand and charge the BS for the period between 07:00 and 16:00. The PV and the WT worked hand-in-hand from 07:00 to 16:00. The PV stopped producing power by 17:00, and the BS and the WT worked hand-in-hand to meet the load demand for the rest of the day.

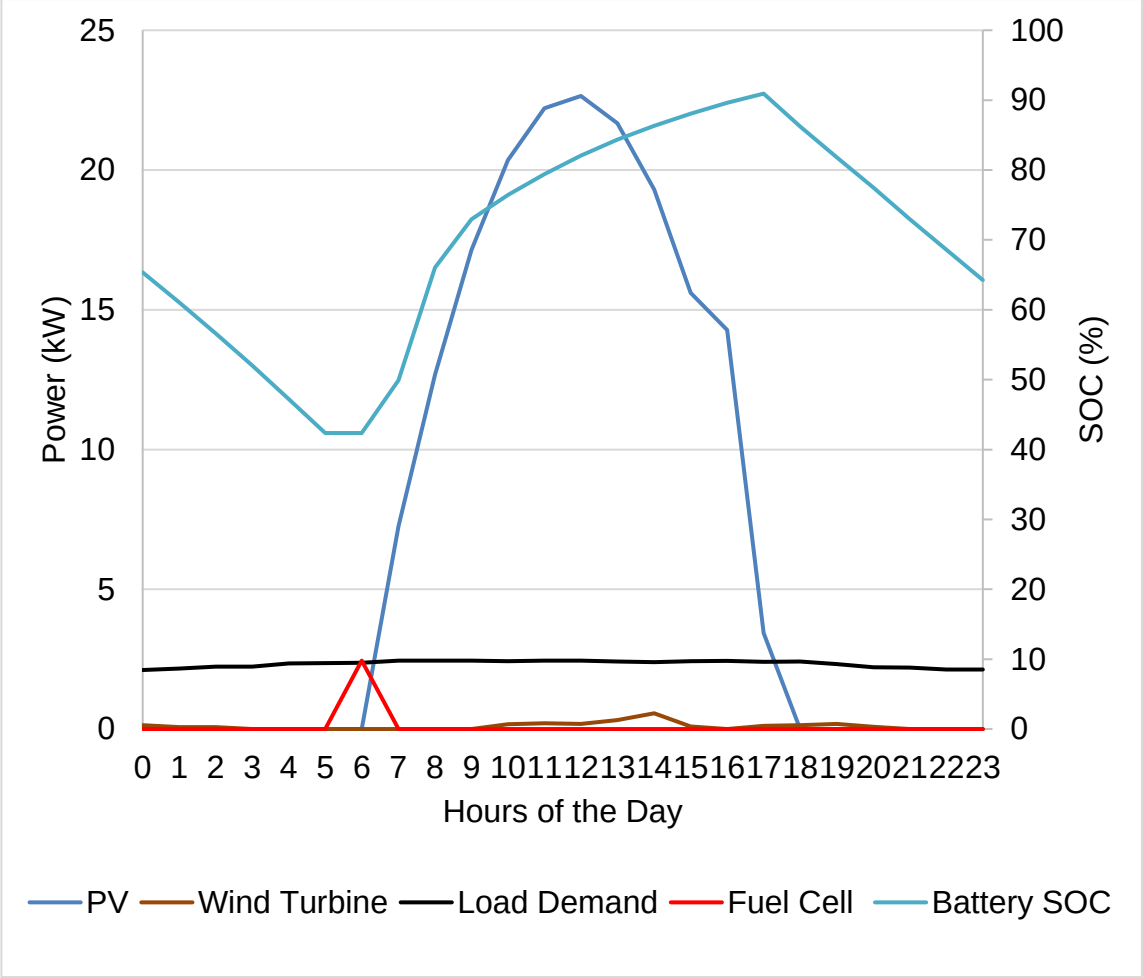

Figure 4. 11. The power flow and the battery SOC in Mafikeng.

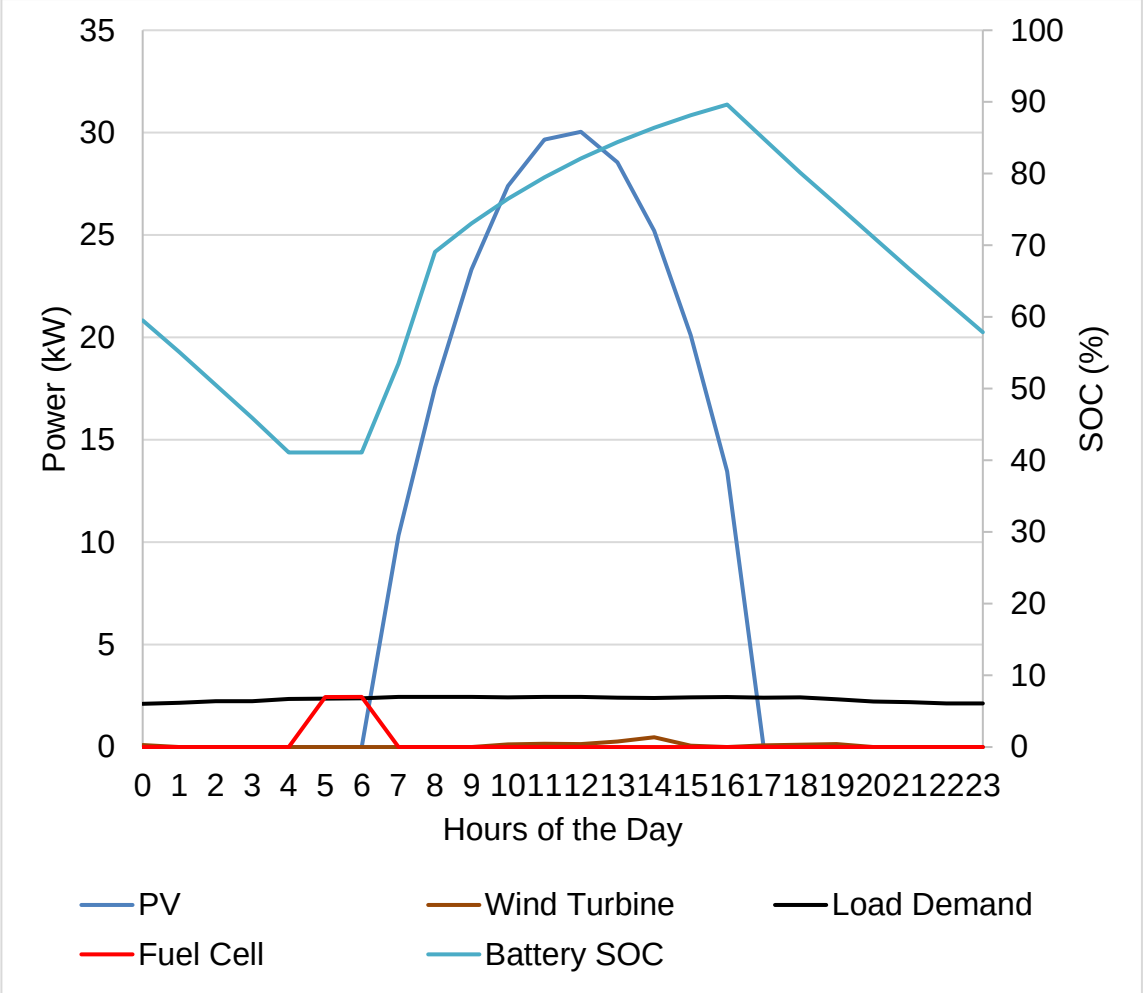

Figure 4. 12. The power flow and the battery SOC in Rustenburg.

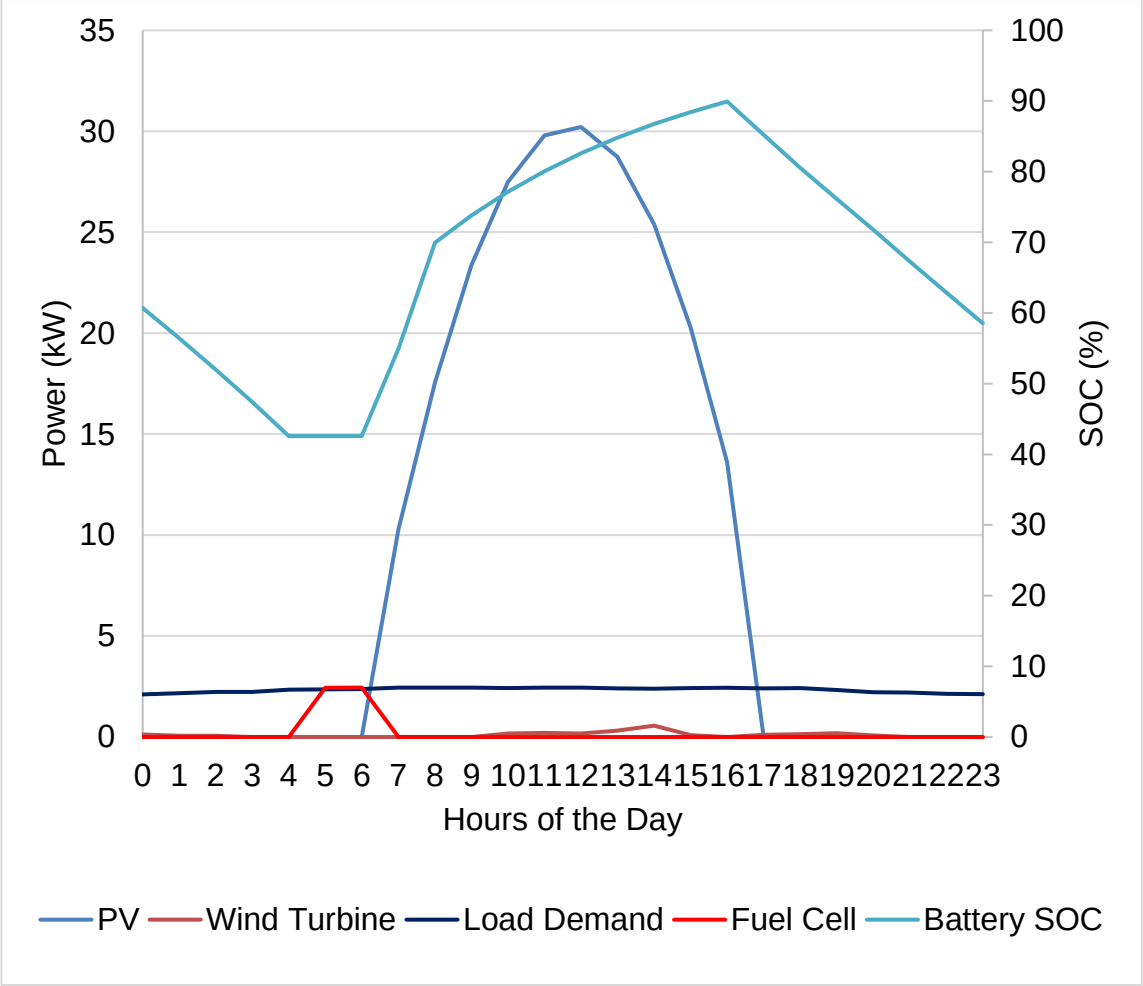

Figure 4. 13. The power flow and the battery SOC in Potchefstroom.

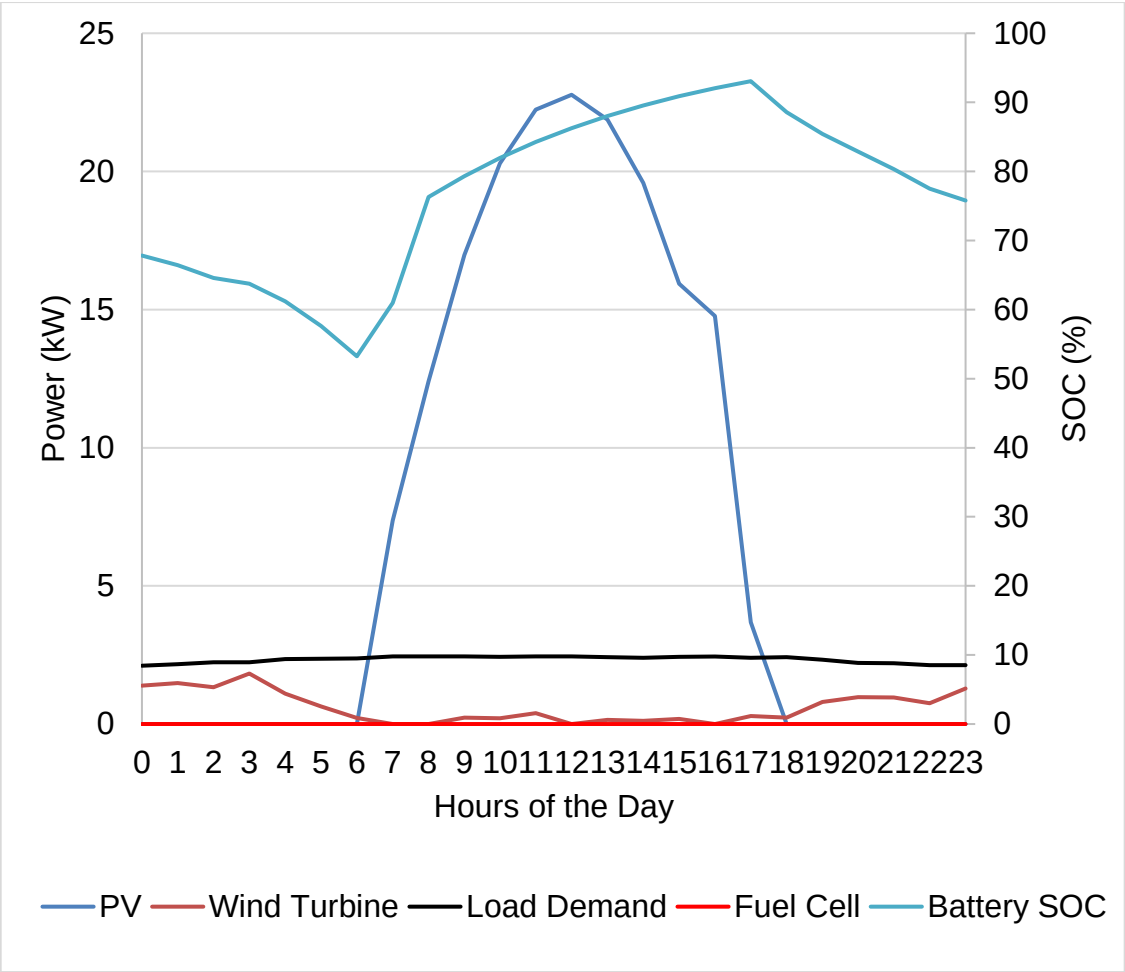

Figure 4. 14. The power flow and the battery SOC in Vryburg.

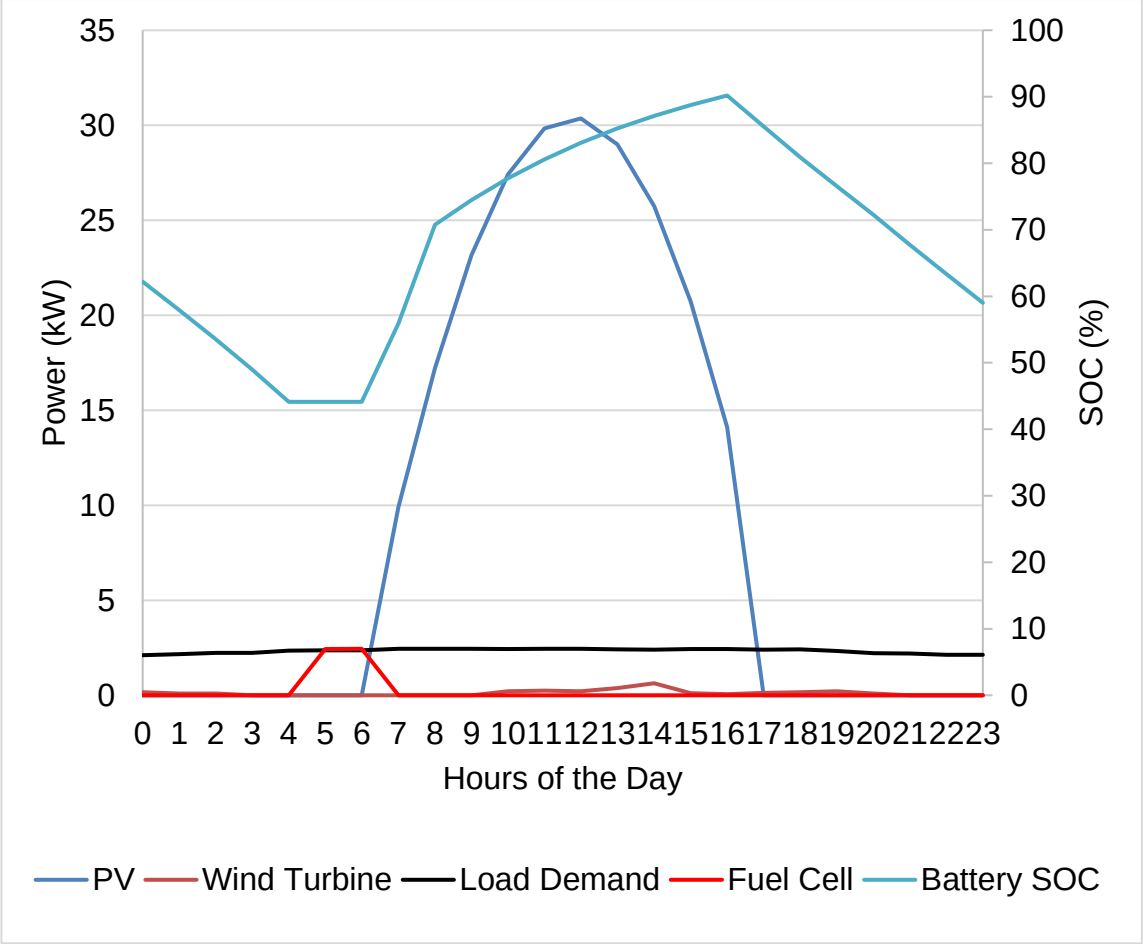

Figure 4. 15. The power flow and the battery SOC in Lichtenburg.

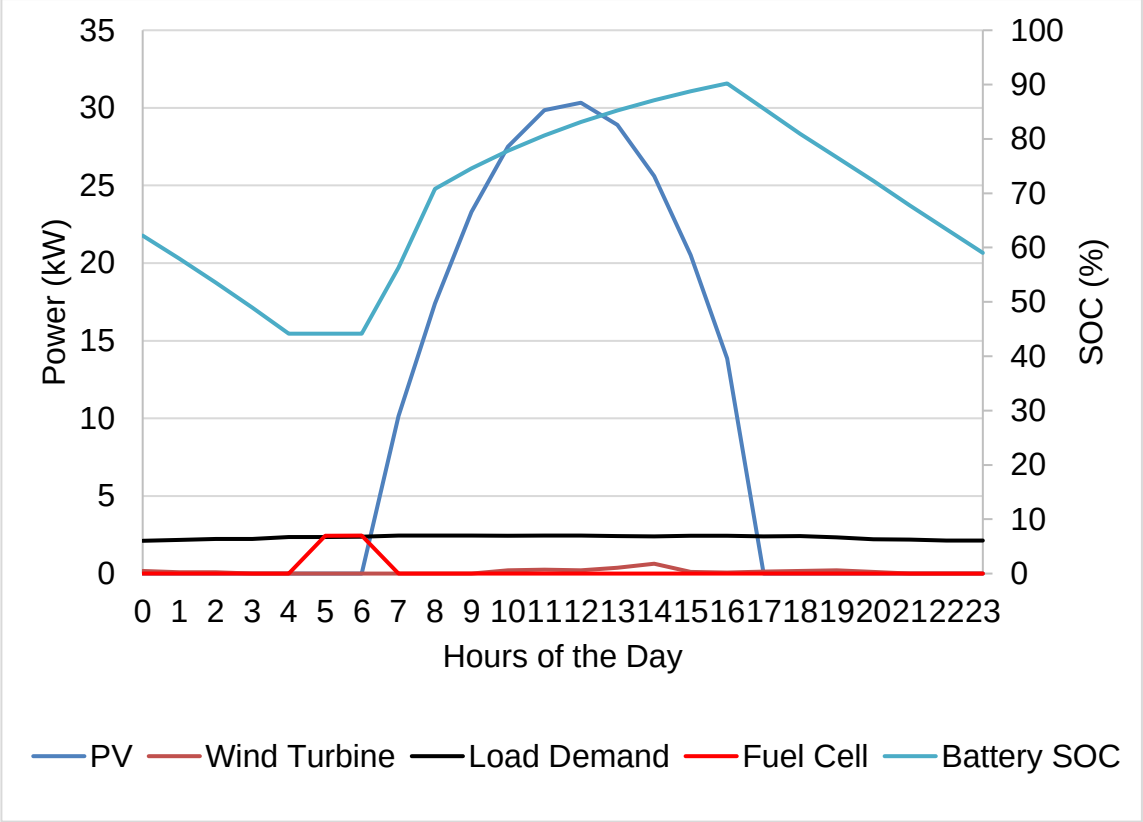

Figure 4. 16. The power flow and the battery SOC in Klerksdorp.

4.6. Summary of the Chapter

The performance of the proposed HRES in all the selected sites has been presented and discussed in this chapter. The results presented in this chapter demonstrated that the RER chosen for the proposed micro-grid system were able to fulfil the load demand of the LTE BTS. The optimisation results demonstrate that the proposed PV/WT/FC/BS HRES does not require any assistance from the grid power to fulfil the LTE BTS load demand for the whole year. From the power flow results analysis, it can be seen that the proposed PV/WT/FC/BS HRES is capable of providing reliable and sufficient energy to the LTE BTS in all sites as it does not have any capacity shortage. Furthermore, the power flow results demonstrated that the LF dispatch strategy worked very well

by keeping the BS between the prescribed minimum SOC and Maximum SOC. From the financial analysis results, it has been seen that the proposed PV/WT/FC/BS HRES has significantly reduced the NPC associated with DG/BS system that is used to power LTE BTSs in remote areas. This confirms that the future aspects of PV/WT/FC/BS are promising. The subsidising of RES components in African countries can speed up RER penetration just like Spain, Germany, and France, who are leading in PV penetration. Finally, the results have shown that the PV/WT/FC/BS HRES can effectively reduce the GHG emissions and the NPC associated with DG/BS systems in rural areas. Chapter 5 presents the conclusions and recommendations of this study.

CONCLUSION AND RECOMMENDATIONS

5.1. Conclusion

The aim of this study as stipulated in the first chapter was to optimally design an HRES that has the potential to generate electrical power that can adequately power an LTE BTS in the rural areas in South Africa. The HRES was simulated in HOMER for six hypothetical LTE BTS sites. The simulation was done to show the performance of the proposed HRES at the selected LTE BTS sites in rural South Africa. The monthly average SI, CI and WS of each site were used to study the effects of different climatic data on the optimisation of the HRES. This data was used as some of the input variables to run the optimisation process in order to generate optimisation results. The HOMER simulation results demonstrated that out of 20480 simulations only seven hybrid configurations were feasible according to the constraints stipulated. The optimisation results were ranked according to the NPC of each HRES. From the optimisation results, the proposed PV/WT/FC/BS HRES results were compared to the DG/BS system currently used to power LTE BTSs in rural areas of South Africa. The two systems were compared with regard to the NPC, GHG emissions, RF and system capacity shortage. The life-span of both systems was considered to be 25 years. Moreover, the appealing NPC cost and the GHG emissions of the system aided in the selection of the HOMER optimisation model. The NPC for the PV/WT/FC/BS HRES was found to be 63% less than that of the DG/BS system, while the GHG emissions were found to be reduced by as much as 100% by the proposed HRES. Furthermore, the RF was increased by 100% and the system capacity shortage was reduced by 100%. However, it must be noted that the analysis of costs in this work included the emissions costs and the actual per unit kWh cost in South Africa. Within 10 months, the yield regarding the financial expenditure was discovered to be beneficial.

In summary, the proposed HRES can power the LTE BTS in a more cost-effective, environmentally-friendly and a reliable way in comparison to DG/BS systems. Also, the proposed HRES can be effectively implemented for application in places that have no access to the national grid like the rural areas. However, in using RESs for powering the LTE BTS in different sites, it should be noted that there is no general least-cost option. This is because the HRES is heavily reliant on the availability of the RERs and the climatic conditions. The study, therefore, concludes that the proposed PV/WT/FC/BS HRES is the most feasible, cost-effective and environmentally-friendly system when compared to the DG/BS system currently used to power the LTE BTS in the rural areas of South Africa. This conclusion was reached in relation to the power flow, RF, system capacity shortage, reduced NPC and GHG emissions. This also means that the telecommunication operators will be spending less on the costs of the system and they would be helping in the reduction of GHG emissions, which in-turn will help in elevating the global warming epidemic. Cast in this way, the improved reliability will ensure great QoS to the subscribers.

5.2. Future Recommendations

The following are the recommendations from this study:

- Based on the study, there is an abundance of RERs at the chosen study site which can be used to power nearby LTE BTS.
- The RERs can also be used to design an HRES to power a water pumping system that can be used to provide tap water for the households that do not have running water.
- The mapping and prediction of RES in all other locations can be carried out to ensure that the optimal micro-grids are designed and chosen for any application.

- More measurement equipment of SI and WS need to be installed in remote areas for comparison of ground data with satellite radar data.

- There should be security measures in place to mitigate against vandalism and theft of the LTE BTS and micro-grid equipment.

Since most remote places do not have ground data measuring meteorological stations to measure the daily atmospheric data required for the optimisation of HRESs [64], this study recommends the use an of Principal Component Analysis (PCA) and ANN prediction model to predict the SI and WS of those places for future evaluation and development of PV and WT RES. The prediction model designed in this study will help engineers to predict the SI and WS to design and implement the off-grid-connected PV and WT RESs in remote or rural communities. The PCA was used to reduce the dimensions of the measured data and the ANN was used for prediction of the SI [65]. The network used in this study is shown in Figure 5.1, while the training parameters that were used to train the network are presented in Table 5.1.

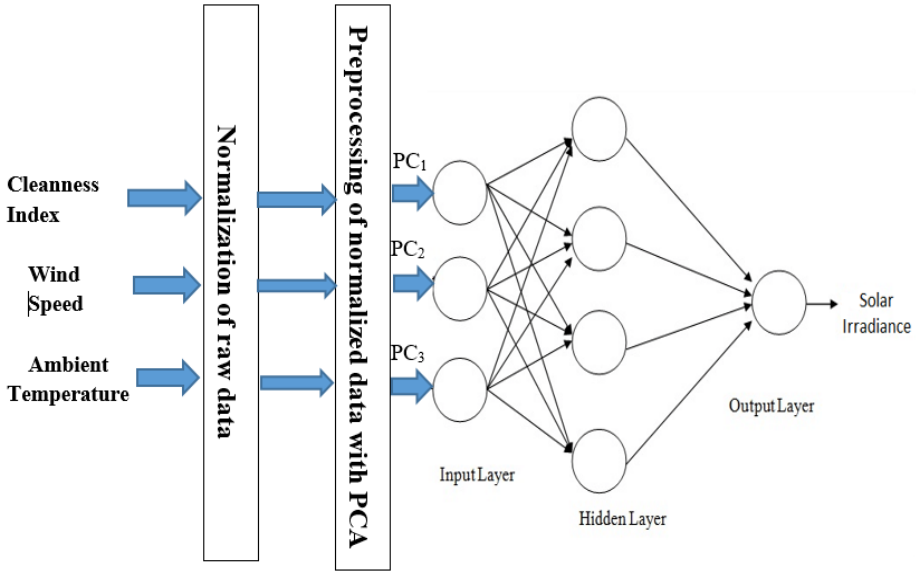

Figure 5. 1. The architecture of the ANN network used in this study.

Table 5. 1. Training parameters of the selected training algorithm.

Generate command-line output	False
Show training GUI	True
Maximum mu	1e10
Mu decrease factor	0.1
Mu increase factor	10
Epochs between displays	25
Initial mu	0.001
Maximum time to train in seconds	Inf
Maximum validation failures	6
Minimum performance gradient	1e−5
Maximum number of epochs to train	1000
Performance goal	0

The MATLAB code utilised to model the PCA+ANN model to predict the monthly daily average SI is presented in ANNEXURE A-11.

The Levenberg-Marquardt (LM) training algorithm was used for training the network. The chosen activation function in the hidden layer was the sigmoid function. Training and validation of the ANN model were performed with different numbers of neurons. The optimal number of hidden layer neurons was found to be 10. The input layer of the ANN model had 3 PCs as the input variables which represented the monthly daily average AT, WS and CI. In the output layer, there was only one neuron, the monthly daily average SI variable. The entire dataset, which consisted of 468 data points was randomly divided into 60% for training, 20% for testing, and 20% for validation, respectively.

The ANN model was trained with all the variables in the dataset and the ANN+PCA model was trained with PCA chosen variables. This was done to show whether the PCA has improved the prediction accuracy of the ANN model. The Root Mean Square Error (RMSE) and the coefficient of determination (R^2) were used to validate the ANN model and the proposed ANN+PCA model. The performance results from the two models are presented in Table 4.5. It can be seen from Table 4.5 that the PCA+ANN model performed better than the ANN only model. The results show that the predicted SI fits the actual SI data by as much as 89.16%. These results further show that the PCA improved the ANN results by as much as 4.63%. Furthermore, the PCA reduced the RMSE by as much as 17.2%. This shows that the SI data predicted, using the PCA+ANN model, could be used in the HOMER simulation process.

Table 5. 2. Performance results of the ANN and ANN+PCA models.

Metric	ANN	PCA+ANN
R^2	84.53%	89.16%
RMSE	0.64	0.53

Figure 5.2 shows the comparison of the measured SI, ANN model predicted SI and the ANN+PCA model predicted SI. From Figure 4.2, it can be seen that the prediction accuracy of the ANN+PCA model is higher than that of the ANN model. The predicted SI values from the ANN+PCA model are a lot closer to the measured SI values as confirmed by Figure 3.8 and the R^2 and RMSE with values of 89.16% and 0.53.

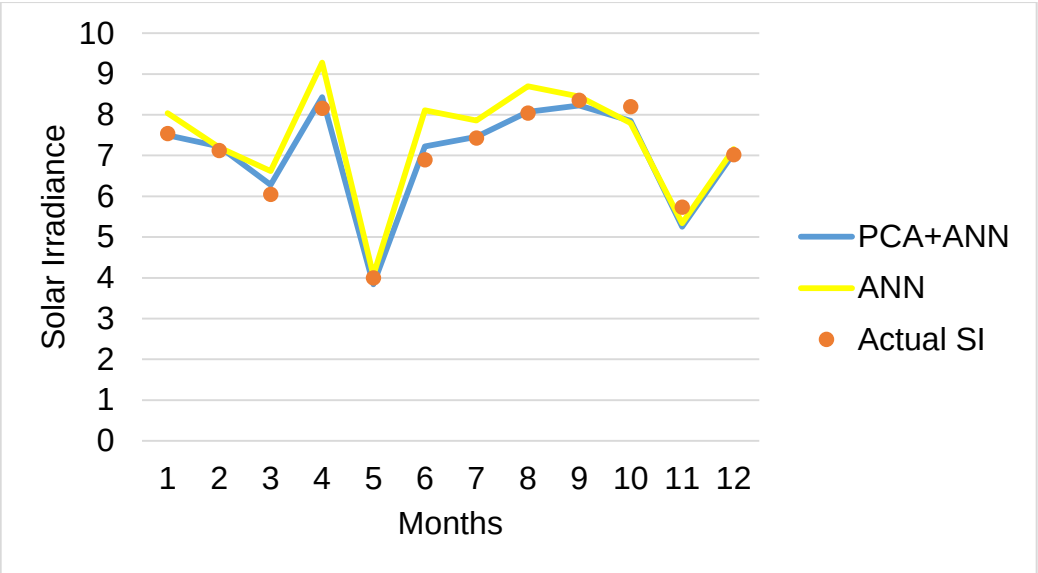

Figure 5. 2. Comparison of the two prediction methods.

From the prediction results, it can be seen that the recommended prediction model can help predict the SI in rural and remote areas which in-turn will assist engineers in the prediction of SI for future implementation and optimisation of HRESs in rural or remote areas.

REFERENCES

[1] M. F. Mpwanya and C. H. V. Heerden, “Perceptions of mobile network operators regarding the cost drivers of the South African mobile phone industry,” Acta Commercii, vol. 16, no. 1, Sep. 2016.

[2] P. Nduhuura, A. Zerga, and M. Garschagen, “Power Outages in Africa – An Assessment Based on Regional Power Pools,” SSRN Electronic Journal, 2018.

[3] P. P. Kumar, G. S. Sarma, and R. P. Kumar, “Barriers for Implementation of Renewable Energy Technologies in Rural Areas-a Review,” International Journal of Trend in Scientific Research and Development, vol. Volume-1, no. Issue-6, pp. 942–945, 2017.

[4] Y. Mekonnen and A. I. Sarwat, “Renewable energy supported microgrid in rural electrification of Sub-Saharan Africa,” 2017 IEEE PES PowerAfrica, 2017.

[5] P. Moriarty and D. Honnery, “Global renewable energy resources and use in 2050,” Managing Global Warming, pp. 221–235, 2019.

[6] C. Vogel and M. Swilling, “Climate change and vulnerability in South Africa,” Sustainability Transitions in South Africa, pp. 40–57, Nov. 2018.

[7] B. Bossoufi, M. Lamnadi, M. Trihi, and A. Boulezhar, “Optimal design of stand-alone hybrid power system using wind and solar energy sources,” International Journal of Energy Technology and Policy, vol. 15, no. 2/3, p. 280, 2019.

[8] A. Yahya, “Opportunities, Challenges, and Terms Related to LTE-A Cellular Network,” LTE-A Cellular Networks, pp. 5–40, Mar. 2016.

[9] B. Shah, G. Dalwadi, H. Shah, and N. Kothari, “Energy-Efficient LTE Access Network For Rural And Remote Areas,” Far East Journal of Electronics and Communications, vol. 18, no. 7, pp. 1073–1097, 2018.

[10] M. Alsharif and J. Kim, “Optimal Solar Power System for Remote Telecommunication Base Stations: A Case Study Based on the Characteristics of South Korea’s Solar Radiation Exposure,” Sustainability, vol. 8, no. 9, p. 942, 2016.

[11] J. F. G. D. Oliveira and T. C. G. Trindade, “Sustainability Performance Evaluation of Renewable Energy Technologies,” Sustainability Performance Evaluation of Renewable Energy Sources: The Case of Brazil, pp. 77–88, 2018.

[12] A. Aittokallio, “Mobile data traffic to increase ten-fold by 2019 – report,” Telecoms.com, 04-Feb-2015. [Online]. Available: http://telecoms.com/396142/mobile-data-traffic-to-increase-ten-fold-by-2019-report/. [Accessed: 04-Aug-2019].

[13] P. A. Owusu and S. Asumadu-Sarkodie, “A review of renewable energy sources, sustainability issues and climate change mitigation,” Cogent Engineering, vol. 3, no. 1, 2016.

[14] B. Rawn and H. Louie, "Planning for Electrification: On- and Off-Grid Considerations in Sub-Saharan Africa", IDS Bulletin, vol. 48, no. 5-6, 2017. Available: 10.19088/1968-2017.161.

[15] "Is mobile phone tower radiation a health hazard?", Hindustan Times, 2020. [Online]. Available: https://www.hindustantimes.com/health-and-fitness/is-mobile-phone-tower-radiation-a-health-hazard/story-U36Vsl3VpIBQOg043iyvBN.html. [Accessed: 28- March- 2020].

[16] "Natural Gas Generators vs Diesel Generators, Gas Power Generator, Gas Generator | Generator Source", Generatorsource.com, 2020. [Online]. Available:https://www.generatorsource.com/Natural_Gas_vs_Diesel_Generators.aspx. [Accessed: 28- Jun- 2020].

[17] J. Lorincz and I. Bule, "Renewable Energy Sources for Power Supply of Base Station Sites", International Journal of Business Data Communications and Networking, vol. 9, no. 3, pp. 53-74, 2013. Available: 10.4018/jbdcn.2013070104..

[18] M. Alsharif, R. Nordin and M. Ismail, "Energy optimisation of hybrid off-grid system for remote telecommunication base station deployment in Malaysia", EURASIP Journal on Wireless Communications and Networking, vol. 2015, no. 1, 2015. Available: 10.1186/s13638-015-0284-7.

[19] R. Singh and R. Bansal, "Review of HRES's based on storage options, system architecture and optimisation criteria and methodologies", IET Renewable Power Generation, vol. 12, no. 7, pp. 747-760, 2018. Available: 10.1049/iet-rpg.2017.0603.

[20] Y. Sawle, S. Gupta and A. Bohre, "Review of hybrid renewable energy systems with comparative analysis of off-grid hybrid system", Renewable and Sustainable Energy Reviews, vol. 81, pp. 2217-2235, 2018. Available: 10.1016/j.rser.2017.06.033.

[21] S. Singh, M. Singh and S. Kaushik, "A review on optimisation techniques for sizing of solar-wind hybrid energy systems", International Journal of Green Energy, vol. 13, no. 15, pp. 1564-1578, 2016. Available: 10.1080/15435075.2016.1207079.

[22] R. Singh and R. Bansal, "Review of HRES's based on storage options, system architecture and optimisation criteria and methodologies", IET Renewable Power Generation, vol. 12, no. 7, pp. 747-760, 2018. Available: 10.1049/iet-rpg.2017.0603.

[23] A. Al-Shamma'a and K. Addoweesh, "Techno-economic optimization of hybrid power system using genetic algorithm", International Journal of Energy Research, vol. 38, no. 12, pp. 1608-1623, 2014. Available: 10.1002/er.3191.

[24] H. Chen, "Optimum capacity determination of stand-alone hybrid generation system considering cost and reliability", Applied Energy, vol. 103, pp. 155-164, 2013. Available: 10.1016/j.apenergy.2012.09.022.

[25] G. Merei, C. Berger and D. Sauer, "Optimization of an off-grid hybrid PV–Wind–Diesel system with different battery technologies using genetic algorithm", Solar Energy, vol. 97, pp. 460-473, 2013. Available: 10.1016/j.solener.2013.08.016.

[26] Ould Bilal B, "Methodology to Size an Optimal Standalone Hybrid Solar-Wind-Battery System using Genetic Algorithm", International Journal of the Physical Sciences, vol. 7, no. 18, 2012. Available: 10.5897/ijps12.272.

[27] N. Ahmed, H. Farghally and F. Fahmy, "Optimal Sizing and Economical Analysis of PV-Wind Hybrid Power System for Water Irrigation using Genetic Algorithm", International Journal of Electrical and Computer Engineering (IJECE), vol. 7, no. 4, p. 1797, 2017. Available: 10.11591/ijece.v7i4.pp1797-1814.

[28] S. Charfi, A. Atieh and M. Chaabene, "Optimal sizing of a hybrid solar energy system using particle swarm optimisation algorithm based on cost and pollution criteria", Environmental Progress & Sustainable Energy, vol. 38, no. 3, p. e13055, 2018. Available: 10.1002/ep.13055.

[29] O. Mohammed, Y. Amirat and M. Benbouzid, "Particle Swarm Optimization Of a Hybrid Wind/Tidal/PV/Battery Energy System. Application To a Remote Area In Bretagne, France", Energy Procedia, vol. 162, pp. 87-96, 2019. Available: 10.1016/j.egypro.2019.04.010.

[30] M. Amer, A. Namaane and N. M'Sirdi, "Optimization of Hybrid Renewable Energy Systems (HRES) Using PSO for Cost Reduction", Energy Procedia, vol. 42, pp. 318-327, 2013. Available: 10.1016/j.egypro.2013.11.032.

[31] M. Mohamed, A. Eltamaly and A. Alolah, "PSO-Based Smart Grid Application for Sizing and Optimization of Hybrid Renewable Energy

Systems", PLOS ONE, vol. 11, no. 8, p. e0159702, 2016. Available: 10.1371/journal.pone.0159702..

[32] A. Chauhan and V. K. Dwivedi, "Optimal sizing of a stand-alone PV/wind/MHP/biomass-based hybrid energy system using PSO algorithm," 2017 6th International Conference on Computer Applications In Electrical Engineering-Recent Advances (CERA), Roorkee, 2017, pp. 7-12, doi: 10.1109/CERA.2017.8343292.

[33] N. Agarwala, A. Kumarb and Varun, "Sizing Analysis and Cost Optimization of Hybrid Solar-Diesel-Battery Based Electric Power Generation System Using Simulated Annealing Technique", Distributed Generation & Alternative Energy Journal, vol. 27, no. 3, pp. 26-51, 2012. Available: 10.1080/21563306.2012.10531122.

[34] O. Ekren and B. Ekren, "Size optimization of a PV/wind hybrid energy conversion system with battery storage using simulated annealing", Applied Energy, vol. 87, no. 2, pp. 592-598, 2010. Available: 10.1016/j.apenergy.2009.05.022.

[35] C. C. Fung, S. C. Y. Ho and C. V. Nayar, "Optimisation of a hybrid energy system using simulated annealing technique," Proceedings of TENCON '93. IEEE Region 10 International Conference on Computers, Communications and Automation, Beijing, China, 1993, pp. 235-238 vol.5, doi: 10.1109/TENCON.1993.320626.

[36] P. Suhane, S. Rangnekar, A. Khare and A. Mittal, "Sizing and performance analysis of standalone wind-photovoltaic based hybrid energy system using ant colony optimisation", IET Renewable Power

Generation, vol. 10, no. 7, pp. 964-972, 2016. Available: 10.1049/iet-rpg.2015.0394.

[37] R. Vijay, "Optimal Placement And Sizing of Wind-Pv Integrated Power Generation By Ant Colony Optimization Technique", International Journal of Recent Trends in Engineering and Research, vol. 3, no. 5, pp. 481-492, 2017. Available: 10.23883/ijrter.2017.3253.luag2.

[38] A. Askarzadeh, "Application of Ant Colony Optimization (ACO) for Designing a Hybrid System", International Journal Of Engineering & Applied Sciences, vol. 6, no. 2, pp. 52-52, 2014. Available: 10.24107/ijeas.251221.

[39] A. Maleki, M. Khajeh and M. Ameri, "Optimal sizing of a grid-independent hybrid renewable energy system incorporating resource uncertainty, and load uncertainty", International Journal of Electrical Power & Energy Systems, vol. 83, pp. 514-524, 2016. Available: 10.1016/j.ijepes.2016.04.008..

[40] Y. Katsigiannis, P. Georgilakis and E. Karapidakis, "Hybrid Simulated Annealing–Tabu Search Method for Optimal Sizing of Autonomous Power Systems With Renewables", IEEE Transactions on Sustainable Energy, vol. 3, no. 3, pp. 330-338, 2012. Available: 10.1109/tste.2012.2184840.

[41] T. Khatib, A. Mohamed and K. Sopian, "Optimization of a PV/wind micro-grid for rural housing electrification using a hybrid iterative/genetic algorithm: A case study of Kuala Terengganu, Malaysia", Energy and Buildings, vol. 47, pp. 321-331, 2012. Available: 10.1016/j.enbuild.2011.12.006..

[42] A. Mellit, S. Kalogirou and M. Drif, "Application of neural networks and genetic algorithms for sizing of photovoltaic systems", Renewable Energy, vol. 35, no. 12, pp. 2881-2893, 2010. Available: 10.1016/j.renene.2010.04.017..

[43] S. Sinha and S. Chandel, "Review of software tools for hybrid renewable energy systems", Renewable and Sustainable Energy Reviews, vol. 32, pp. 192-205, 2014. Available: 10.1016/j.rser.2014.01.035.

[44] N. Chowdhury, C. Akram Hossain, M. Longo and W. Yaïci, "Feasibility and Cost Analysis of Photovoltaic-Biomass Hybrid Energy System in Off-Grid Areas of Bangladesh", Sustainability, vol. 12, no. 4, p. 1568, 2020. Available: 10.3390/su12041568.

[45] J. McGowan, J. Manwell, C. Avelar and C. Warner, "Hybrid wind/PV/diesel hybrid power systems modelling and South American applications", Renewable Energy, vol. 9, no. 1-4, pp. 836-847, 1996. Available: 10.1016/0960-1481(96)88412-6.

[46] Y. Garcia, O. Diaz and R. Guzman, "Design and optimisation of PV/diesel hybrid power system in a hotel", International Journal of Energy Production and Management, vol. 2, no. 1, pp. 52-59, 2017. Available: 10.2495/eq-v2-n1-52-59.

[47] L. Halabi, S. Mekhilef, L. Olatomiwa and J. Hazelton, "Performance analysis of hybrid PV/diesel/battery system using HOMER: A case study Sabah, Malaysia", Energy Conversion and Management, vol. 144, pp. 322-339, 2017. Available: 10.1016/j.enconman.2017.04.070.

[48] A.S Aziz, MFN Tajuddin, MR Adzman, MAM Ramli, "Feasibility analysis of PV/Diesel/battery hybrid energy system using multi-year module", International Journal of Renewable Energy Research, December 2018;8:4.

[49] S. Sigarchian, A. Malmquist and T. Fransson, "Modeling and Control Strategy of a Hybrid PV/Wind/Engine/Battery System to Provide Electricity and Drinkable Water for Remote Applications", Energy Procedia, vol. 57, pp. 1401-1410, 2014. Available: 10.1016/j.egypro.2014.10.087.

[50] L. J. Olatomiwa, S. Mekhilef and A. S. N. Huda, "Optimal sizing of hybrid energy system for a remote telecom tower: A case study in Nigeria," 2014 IEEE Conference on Energy Conversion (CENCON), Johor Bahru, 2014, pp. 243-247, doi: 10.1109/CENCON.2014.6967509.

[51] S. Arefin and N. Das, "Optimized Hybrid Wind-Diesel Energy System with Feasibility Analysis", Technology and Economics of Smart Grids and Sustainable Energy, vol. 2, no. 1, 2017. Available: 10.1007/s40866-017-0025-6.

[52] Q. Hassan, M. Jaszczur and J. Abdulateef, "Optimization of PV/WIND/DIESEL Hybrid Power System in HOMER for Rural Electrification", Journal of Physics: Conference Series, vol. 745, p. 032006, 2016. Available: 10.1088/1742-6596/745/3/032006.

[53] S. Goel and S. Ali, "Hybrid energy systems for off-grid remote telecom tower in Odisha, India", International Journal of Ambient Energy, vol. 36, no. 3, pp. 116-122, 2013. Available: 10.1080/01430750.2013.823110.

[54] "North West Province Hybrid Physical / Political Map", Sa-venues.com, 2020. [Online]. Available: https://www.sa-venues.com/maps/northwestprovince/physical.php. [Accessed: 08- Jul- 2020].

[55] P. Stackhouse, "NASA POWER | Data Access Viewer", Power.larc.nasa.gov, 2020. [Online]. Available: https://power.larc.nasa.gov/data-access-viewer/. [Accessed: 08- Jul- 2020].

[56] G. Auer et al., D2.3: Energy efficiency analysis of the reference systems, areas of improvements and target breakdown. INFSO-ICT-247733 EARTH, ver. 2.0, 2012. [Online]. Available: http://www.ict-earth.eu. [Accessed: 08- Jul- 2020].

[57] "Wind/solar/diesel system GSM mast (Kenya) - The Off-Grid Factory", The Off-Grid Factory, 2020. [Online]. Available: https://www.theoffgridfactory.com/en/project/windzondiesel-systeem-gsm-mast-kenya/. [Accessed: 08- Jul- 2020].

[58] "Welcome to HOMER", Homerenergy.com, 2020. [Online]. Available: https://www.homerenergy.com/products/pro/docs/latest/index.html. [Accessed: 08- Jul- 2020].

[59] “Canadian Solar 405W Super High Power Poly PERC HiKU with MC4,” ThePowerStore.[Online].Available:https://thepowerstore.co.za/products/canadian-solar-405w-super-high-power-poly-perc-hiku-with-mc4. [Accessed: 08- Jul- 2020].

[60] Australianwindandsolar.com, 2020. [Online]. Available: https://www.australianwindandsolar.com/aws-hc-wind-turbines. [Accessed: 08- Jul- 2020].

[61] “fuelcellstore.” Horizon 2000W PEM Fuel Cell [Online]. Available: https://www.fuelcellstore.com/horizon-2000watt-fuel-cell-h-2000. [Accessed: 08- Jul- 2020].

[62] “Trojan T-105-RE Flooded 6V 225Ah Battery,” Solaris. [Online]. Available: https://www.solaris-shop.com/trojan-t-105-re-flooded-6v-225ah-battery/.[Accessed: 08- Jul- 2020].

[63] "Solax X3 Hybrid 10.0-T 3ph 10kW Solar Inverter | SolaX X1-Hybrid HV", 0Bills, 2020. [Online]. Available: https://zerohomebills.com/product/solax-x3-hybrid-10-0-t-3ph-10kw-solar-inverter/. [Accessed: 08- Jul- 2020].

[64] S. Ayobami, O. Adegoke and y. sanusi, "Application of Artificial Neural Network to Predict Annual Global Solar Radiation for PV System’s Sizing in UUM Area, Malaysia.", Academia.edu, 2020. [Online]. Available: https://www.academia.edu/10351365/Application_of_Artificial_Neural_Network_to_Predict_Annual_Global_Solar_Radiation_for_PV_System_s_Sizing_in_UUM_Area_Malaysia. [Accessed: 06- Aug- 2020].

[65] F. Taşpınar, “Improving artificial neural network model predictions of daily average PM10 concentrations by applying principle component analysis and implementing seasonal models,” Journal of the Air & Waste Management Association, vol. 65, no. 7, pp. 800–809, 2015.

[66] A. Ayang, P.-S. Ngohe-Ekam, B. Videme, and J. Temga, “Power Consumption: Base Stations of Telecommunication in Sahel Zone of

Cameroon: Typology Based on the Power Consumption—Model and Energy Savings," Journal of Energy, vol. 2016, pp. 1–15, 2016.

[67] T. Huld and A. Amillo, "Estimating PV Module Performance over Large Geographical Regions: The Role of Irradiance, Air Temperature, Wind Speed and Solar Spectrum," Energies, vol. 8, no. 6, pp. 5159–5181, Feb. 2015.

ANNEXURE A-1: MATLAB Code for PV Panel Model

```
%HiKu SUPER HIGH POWER POLY PERC MODULE PV_Characteristics

clc;
close all;
clear all;

        %Constants used in the modelling of the PV panel

T=302;                      %Operating Temperature
Tr=298;                     %Temperature at STC
Tr1=40;
Ki=0.05;            %Short Circuit Current of Cell at 25º and 1000 W/m2
Iscr=10.98;                 %Short Circuit Current
Irr=0.000021;       %Diode reverse saturation current
A=2.15;                     %The diode ideality factor
Ego=1.166;    %gap energy of semiconductor at zero Kelvin
alpha=0.473;          %Temperature Coefficient of Iscr
beta=636;             %Temperature Coefficient of Voc
G=[100 80 60 40 20];              %Solar Irradiance
k=1.38065*10^(-23);               %Boltzman Constant
q=1.6022*10^(-19);            %Charge of an electron
Eg=Ego-(alpha*T*T)/(T+beta)*q;%gap energy of semiconductor
Np=4;               %Number of Parallel Conected Cells
Ns=60;                    %Number of Series Connected Cells
Voc=(0:1:300);        %Desierable Open Circuit Voltage

%Finding values for all five values of sun
```

```
for i=1:5
    Iph=(Iscr+ki*(T-Tr))*((G(i))/100); %Phase current
    Irs=Irr*((T/Tr)^3)*exp(q*Eg/(k*A)*((1/Tr)-(1/T))); %Current through shunt
resistor
    Iout=Np*Iph-Np*Irs*(exp (q/ (k*T*A)*Voc. /Ns)-1); %Output Current
    Pout=Voc.*Iout; %Output power
    figure (1) % voltage vs current plot
    plot(Voc,Iout);
    axis([0 50 0 50]);
    xlabel('Voltage in Volts');
    ylabel('Current in Amps');
    hold on;
    figure(2) % voltage vs power plot
    plot(Voc,Pout);
    axis([0 50 0 1600]);
    xlabel('Voltage in Volts');
    ylabel('Power in Watts');
    hold on;
    figure(3) % current vs power plot
    plot(Iout,Pout);
    axis([0 50 0 1600]);
    xlabel('Current in Amps');
    ylabel('Power in Watts');
    hold on;
end
```

ANNEXURE A-2: MATLAB Code for WT Model

```
%Initialisation of the lookup table
WSds = transpose (2:0.5:12);
WPds = [23;45;78;123;185;263;361;481;624;794;991;1219;1480;1775;2108;2
479; 2891; 3050; 3120; 3150; 3150];
%Declaring the input parameters
x= WSds;
y= WPds;
%Polyfitting the data
p = polyfit(x, y, 4);
%Plotting the wind power curve
x1 = linspace(0,4*pi);
y1 = polyval (p, x1);
figure
plot(x, y,'o')
hold on
plot(x1, y1)
hold off
```

where

WSds and WPds represent the WS and WP data supplied by the manufactures datasheet. The WSdsint and WPdsint represent the interpolated data with values at every 0.1 interval.

ANNEXURE A-3: MATLAB Code for the Battery Current Profile

```
%Initialisation of the lookup table

CPds = [247 206 182 153 135 118 96 60]; % Capacity from datasheet
CUds = [2.1 11 27.5 50 75 100 150 250];%Current

%Declaring the input parameters

x= CPds;
y= CUds;

%Polyfitting the data

p = polyfit(x, y, 4);

%Plotting the capacity/discharge current profile

x1 = linspace(0,4*pi);
y1 = polyval (p, x1);
figure
plot(x, y,'o')
hold on
plot(x1, y1)
hold off
```

where
CPds and CUds represent the battery capacity and current data supplied by the manufactures datasheet.

ANNEXURE A-4: MATLAB Code for Fuel Consumption Profile of the FC

```
%Initialisation of the lookup table

FCds = [0; 4,9; 9,9; 15; 21; 28; 37]; % Fuel consumption from datasheet
OPds = [0; 0.5; 1; 1.5; 2; 2.5; 3];%Output Power from datasheet

%Declaring the input parameters

x= FCds;
y= OPds;

%Polyfitting the data

p = polyfit(x, y, 2);

%Plotting the fuel consumption/output power profile

x1 = linspace(0,4*pi);
y1 = polyval (p, x1);
figure
plot(x, y,'o')
hold on
plot(x1, y1)
hold off
```

where

FCds and OPds represent the FC fuel consumption and output power data supplied by the manufactures datasheet.

ANNEXURE A-5: MATLAB Code for DG Model

```
%Initialisation of the lookup table
OPds = transpose(0:2.5:10);
FCds = [0.49;1.58;2.65;3.8;4.83];
%Declaring the input parameters
x= OPds;
y= FCds;
%Polyfitting the data
p = polyfit(x, y, 1);
%Plotting the Fuel-Power curve
x1 = linspace(0,4*pi);
y1 = polyval (p, x1);
figure
plot(x, y,'o')
hold on
plot(x1, y1)
hold off
```

where

OPds and FCds represent the output power and FC fuel consumption data supplied by the manufactures datasheet.

ANNEXURE A-6: HiKU CS3W-390-405P PV panel Datasheet

ENGINEERING DRAWING (mm)

Rear View

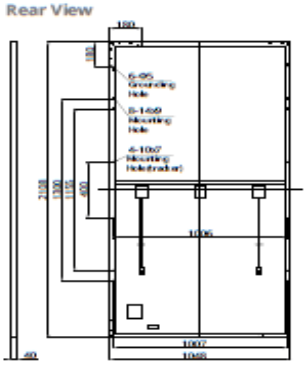

Frame Cross Section A-A

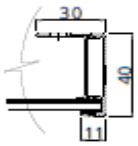

Mounting Hole

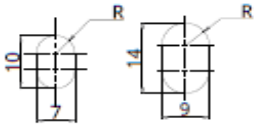

CS3W-400P / I-V CURVES

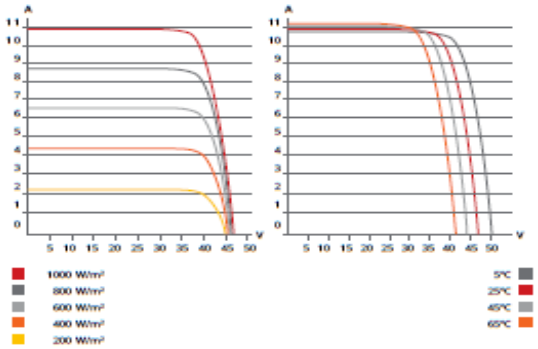

ELECTRICAL DATA | STC*

CS3W	390P	395P	400P	405P
Nominal Max. Power (Pmax)	390 W	395 W	400 W	405 W
Opt. Operating Voltage (Vmp)	38.3 V	38.5 V	38.7 V	38.9 V
Opt. Operating Current (Imp)	10.19 A	10.26 A	10.34 A	10.42 A
Open Circuit Voltage (Voc)	46.8 V	47.0 V	47.2 V	47.4 V
Short Circuit Current (Isc)	10.74 A	10.82 A	10.90 A	10.98 A
Module Efficiency	17.65%	17.88%	18.11%	18.33%
Operating Temperature	-40°C ~ +85°C			
Max. System Voltage	1500V (IEC/UL) or 1000V (IEC/UL)			
Module Fire Performance	TYPE 1 (UL 1703) or CLASS C (IEC 61730)			
Max. Series Fuse Rating	20 A			
Application Classification	Class A			
Power Tolerance	0 ~ + 5 W			

* Under Standard Test Conditions (STC) of irradiance of 1000 W/m², spectrum AM 1.5 and cell temperature of 25°C.

ELECTRICAL DATA | NMOT*

CS3W	390P	395P	400P	405P
Nominal Max. Power (Pmax)	290 W	293 W	297 W	301 W
Opt. Operating Voltage (Vmp)	34.9 V	35.1 V	35.3 V	35.5 V
Opt. Operating Current (Imp)	8.31 A	8.35 A	8.42 A	8.48 A
Open Circuit Voltage (Voc)	43.8 V	44.0 V	44.2 V	44.4 V
Short Circuit Current (Isc)	8.67 A	8.72 A	8.78 A	8.85 A

* Under Nominal Module Operating Temperature (NMOT), irradiance of 800 W/m² spectrum AM 1.5, ambient temperature 20°C, wind speed 1 m/s.

MECHANICAL DATA

Specification	Data
Cell Type	Poly-crystalline
Cell Arrangement	144 [2 X (12 X 6)]
Dimensions	2108 X 1048 X 40 mm (83.0 X 41.3 X 1.57 in)
Weight	24.9 kg (54.9 lbs)
Front Cover	3.2 mm tempered glass
Frame	Anodized aluminium alloy, crossbar enhanced
J-Box	IP68, 3 bypass diodes
Cable	4 mm² (IEC), 12 AWG (UL)
Cable Length (Including Connector)	1400 mm (55.1 in), 1700 mm (66.9 in) is optional for single tracking system with leap-frog connection
Connector	T4 series
Per Pallet	27 pieces
Per Container (40' HQ)	594 pieces

TEMPERATURE CHARACTERISTICS

Specification	Data
Temperature Coefficient (Pmax)	-0.37 % / °C
Temperature Coefficient (Voc)	-0.29 % / °C
Temperature Coefficient (Isc)	0.05 % / °C
Nominal Module Operating Temperature	42 ± 3°C

PARTNER SECTION

* The specifications and key features contained in this datasheet may deviate slightly from our actual products due to the on-going innovation and product enhancement. Canadian Solar Inc. reserves the right to make necessary adjustment to the information described herein at any time without further notice.

CANADIAN SOLAR INC.
545 Speedvale Avenue West, Guelph, Ontario N1K 1E6, Canada, www.canadiansolar.com, support@canadiansolar.com

ANNEXURE A-7: The Kestrel e400n 3.5 kW Datasheet

EVEREADY kestrel wind turbines

kestrel

Small Wind Turbine Class	II
Rated Output	3000w
Maximum Power	3300w at 12ms^{-1}
Rated Wind speed	11ms^{-1}
Cut-in Wind speed	2.8ms^{-1}
Generator Type	Permanent-magnet Axial flux brushless
Rotor Diameter	4m
Number of Blades	3
Blade Material	Fibre glass
Tower Top Mass	150kg
Tower Height	12-15m
Tower Type	Tripod
Overspeed Protection	Pitch Control
Controller Type	Charge ONLY
Output Voltage	48*,200 and 300 Vdc
Application	Battery-charging
	Grid Tie
	Hybrid
	Water Pumping

*Available on request

Technical Specifications

Rated output is achieved at the rated wind speed at sea level. Rated power is the optimal power rating of the turbine at the rated wind speed, making it maintainable without a cut out wind speed.

Rated output is optimised by technology and design, namely by dynamically limiting the output by pitch control. The Axial Flux alternator type reduces the heat losses while energy is being generated in the form of polyphase high frequency output.

The full aerofoil blades are moulded from fibre glass and protected from dust and moisture. The e400i conforms to IEC standards and follows the provisions in the directives IEC61400-2 (small wind turbines).

Kestrel Wind Turbines and its global affiliates and dealers are committed to renewable energy generation as well as reducing the use of fossil fuels. Wind power addresses most of the current issues of present renewable power generation options. Kestrel is continuously developing small wind turbine technology to supply personal or business energy demands.

Kestrel is continuously improving current small wind turbines in the Kestrel range to ensure that the highest quality product is distributed. All Kestrel dealers share these values and are trained to support Kestrel's customers in understanding their power requirements and the local wind resource available to them. Also, to evaluate the turbines in the Kestrel range that best accommodates these requirements, assist installations and advise on maintenance procedures.

Power Generation

Generating your own renewable power is low maintenance as routine maintenance is largely based on visual assessments. Maintenance schedules are designed to suit the local, respective, wind area and power class. With a maximum instantaneous power rating of 3300W, annual energy harvests can exceed 13 600kWh. Energy may be harvested at any different wind speed exceeding cut in speed and rated output is maintained at any wind speed exceeding the rated wind speed through rotor turbulence. Energy output is intrinsically linked to regional wind distribution, topology and altitude as well as tower height. Potential energy harvest is estimated using an average wind speed in order to tailor the most suitable Kestrel wind system to your electrical need.

Results may vary based on wind distribution, topology, tower height and altitude. In order to estimate ones own potential energy harvest an average wind speed must be used.

Note: Specifications may vary with continuing development and innovation.

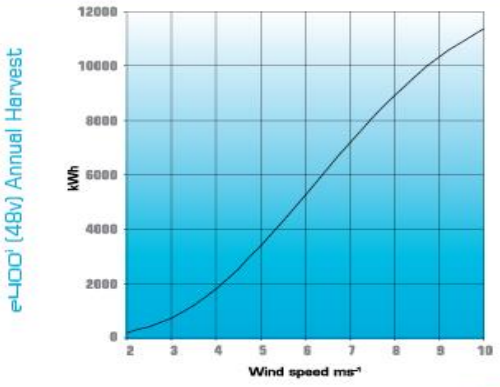

PROUDLY SOUTH AFRICAN CE

Eveready Road, Struandale, Port Elizabeth, 6001, SOUTH AFRICA
PO Box 3191, North End, Port Elizabeth, 6056, SOUTH AFRICA
Tel: +27 (0) 41 401 2500 / 2599 • Fax: +27 (0) 41 394 8183
e-mail: kestrelwind@eveready.co.za • www.kestrelwind.co.za

renewable power for life

ANNEXURE A-8: Horizon H-3000 PEM FC Datasheet

Horizon Fuel Cell Technologies

4. Technical Specifications

Control electronics included:

Type of fuel cell	PEM
Number of cells	72
Rated Power	3000W
Performance	43.2V @ 70A
H2 Supply valve voltage	12V
Purging valve voltage	12V
Blower voltage	12V
Reactants	Hydrogen and Air
External temperature	5 to 30°C
Max stack temperature	65°C
H2 Pressure	0.45-0.55bar
Hydrogen purity	≧99.995% dry H2
Humidification	self-humidified
Cooling	Air (integrated cooling fan)
Weight (with fan & casing)	15Kg (±200g)
Controller	2.5Kg (±100g)
Dimension	41.8cm x35cm x 18.3cm
Flow rate at max output*	39 L/min
Start up time	≦30S at ambient temperature
Efficiency of stack	40% @ 43.2V
Low voltage shut down	36V
Over current shut down	90A
Over temperature shut down	65°C
External power supply**	13V(±1V), 5A~8A

** The flow rate may change with the power output*
*** System electronics need external power supply*
**** The Specification is subject to change without notice.*

ANNEXURE A-9: Trojan T-105 (6V-225 Ah) Battery Datasheet

PRODUCT SPECIFICATIONS

BCI GROUP SIZE	TYPE	CAPACITY[A] Amp-Hours (AH)							ENERGY (kWh)	VOLTAGE	TERMINAL Type[D]	DIMENSIONS[B] Inches (mm)			WEIGHT lbs. (kg)
		2-Hr Rate	5-Hr Rate	10-Hr Rate	20-Hr Rate	48-Hr Rate	72-Hr Rate	100-Hr Rate	100-Hr Rate			Length	Width	Height[C]	
PREMIUM LINE - DEEP-CYCLE FLOODED BATTERIES															
GC2H	T-105 RE	146	185	207	225	240	245	250	1.50	6 VOLT	5	10.30 (262)	7.11 (181)	11.67 (296)	67 (30)

CHARGING INSTRUCTIONS

CHARGER VOLTAGE SETTINGS (AT 77°F/25°C)	
	Voltage per cell
Absorption charge	2.35-2.45
Float charge	2.20
Equalize charge	2.58

Do not install or charge batteries in a sealed or non-ventilated compartment. Constant under or overcharging will damage the battery and shorten its life as with any battery.

TERMINAL CONFIGURATIONS

5 LT	L-Terminal
	*Terminal Height Inches (mm)* 1-3/4 (43) *Torque Values in-lb (Nm)* 100 – 120 (11 – 14) *Bolt* 3/8"

OPERATIONAL DATA

OPERATING TEMPERATURE	SPECIFIC GRAVITY
-4°F to 113°F (-20°C to +45°C). At temperatures below 32°F (0°C) maintain a state of charge greater than 60%.	The specific gravity at 100% state-of-charge is 1.280

Premium Line batteries manufactured prior to March 2012 have 1.260 SG value.

CHARGING TEMPERATURE COMPENSATION

To the Voltage Reading -- Subtract 0.005 volt per cell (VPC) for every 1°C above 25°C or add 0.005 volt per cell for every 1°C below 25°C.

EXPECTED LIFE VS. TEMPERATURE

Chemical reactions internal to the battery are driven by voltage and temperature. The higher the battery temperature, the faster chemical reactions will occur. While higher temperatures can provide improved discharge performance the increased rate of chemical reactions will result in a corresponding loss of battery life. As a rule of thumb, for every 10°C increase in temperature the reaction rate doubles. Thus, a month of operation at 35°C is equivalent in battery life to two months at 25°C. Heat is an enemy of all lead acid batteries, FLA, AGM and gel alike and even small increases in temperature will have a major

T105-RE_

ANNEXURE A-10: Solax X3-hybrid10 10 kW inverter Datasheet

	X1-Hybrid HV (SINGLE PHASE)				X3-Hybrid HV (THREE PHASE)			
	X1-HYBRID-3.0T	X1-HYBRID-3.7T	X1-HYBRID-4.6T	X1-HYBRID-5.0T	X3-Hybrid-5.0T	X3-Hybrid-6.0T	X3-Hybrid-8.0T	X3-Hybrid-10.0T
INPUT (DC)								
Max.recommended DC power[w]	4000	5000	6000	6000	6000	8000	10000	13000
Max.DC voltage[V]	600	600	600	600	1000	1000	1000	1000
Nominal DC operating voltage[V]	360	360	360	360	720	720	720	720
Max.input current[A]	10/10	10/10	10/10	10/10	11/11	11/11	11/11	20/11
Max. short circuit current[A]	14/14	14/14	14/14	14/14	14/14	14/14	14/14	23/14
MPPT voltage range[V]	125-550	125-550	125-550	125-550	230-800	280-800	370-800	330-800
No. of MPP trackers	2	2	2	2	2	2	2	2
Strings per MPP tracker	1	1	1	1	1	1	1	2/1
OUTPUT AC								
Norminal AC power [VA]	3000	3680	4600	4999	5000	6000	8000	10000
Max. AC power [VA]	3000	3680	4600	4999	5000	6000	8000	10000
Rated grid voltage(AC voltage range) [V]	230(180 to 270)	230(180 to 270)	230(180 to 270)	230(180 to 270)	400/360 to 440)	400(360 to 440)	400 (360 to 440)	400 (360 to 440)
Rated grid frequency [Hz]	50/60	50/60	50/60	50/60	50/60	50/60	50/60	50/60
Norminal AC current [A]	13	16	20	21.7	7.6	9	12.2	15
Max. AC current [A]	14.4	16	21	21.7	8.5	10	13.5	16
Displacement power factor	0.8 leading ... 0.8 lagging				0.8 leading ... 0.8 lagging			
Total harmonic distortion(THD, rated power) [%]	<2				<2			
Parallel operation	Yes				Yes			
Load control	Yes (optional)				Yes (optional)			
OUTPUT DC (BATTERY)								
Battery voltage range [V]	85-400				170-500			
Recommended battery voltage [V]	300				200	240	320	400
Max.charging/discharging power [W]	6000				6000	8000	10000	10000
Max.charging/discharging current [A]	20				25			
Communication interfaces	CAN/RS485				CAN/RS485			
Reverse connect protection	Yes				No			
EPS OUTPUT (WITH BATTERY)								
EPS rated power [VA]	4000	4000	5000	5000	5000	6000	8000	10000
EPS rated voltage [V], Frequency [Hz]	230, 50/60	230, 50/60	230, 50/60	230, 50/60	400/380, 50/60	400/380, 50/60	400/380, 50/60	400/380, 50/60
EPS rated current [A]	17.4	17.4	21.7	21.7	7.6	9	12.2	15
EPS peak power[W],Duration [s]	8000,10	8000,10	8000,10	8000,10	10000,60	12000,60	16000,60	16000,60
Switch time[s]	<0.5				<0.5			
Total harmonic distortion(THD, linear load) [%]	<2				<2			
Parallel operation	Yes				Yes			
EFFICIENCY								
MPPT efficiency [%]	99.90	99.90	99.90	99.90	99.90	99.90	99.90	99.90
Euro efficiency [%]	97.00	97.00	97.00	97.00	97.00	97.00	97.00	97.00
Max. efficiency [%]	97.80	97.80	97.80	97.80	97.60	97.60	97.60	97.60
Battery charge/discharge efficiency [%]	98.50	98.50	98.50	98.50	96.00	96.00	96.00	96.00
POWER CONSUMPTION								
Standby consumption(night) [W]	<7				<7			
Idle mode	YES				YES			
STANDARD								
Safety	IEC62109-1-2 / IEC62040				IEC62109-1-2 / IEC62040 / AS3100			
EMC	EN61000-6-1/EN61000-6-2/EN61000-6-3				EN61000-6-1/EN61000-6-2/EN61000-6-3			
Certification	VDE0126-1-1 A1:2012/VDE-AR-N4105/G83/G59/AS4777/EN50438/CEI0-21/VDE2510				VDE0126-1-1 A1:2012/VDE-AR-N4105/G89-3/AS4777/EN50438/CE 0-21/IEC62040/IEC62619/ISO13849-2/SN29500/IEC 61508			
ENVIRONMENT LIMIT								
Protection class	IP65				IP65			
Operating temperature range [°C]	-20 to+60 (derating at+45)				-25 to+60 (derating at+45)			
Altitude[m]	<2000				<2000			
Storage temperature[°C]	-20 to+60				-20 to+60			
Noise emission(typical) [dB]	<30				<30			
Over voltage category	III (electric supply side), II (PV side)				III (electric supply side), II (PV side)			
DIMENSION AND WEIGHT								
Dimensions(WxHxD) [mm]	460*477*181.5				659*458*208			
Weight[kg]	26.9				40			
Cooling concept	Forced-cooling				Forced-cooling			
Topology	Transformerless				Transformerless			
Communication	Ethernet, Meter, WIFI (optional), RF(optional), DRM, USB, ISO alarm, Parallel operation				Ethernet, Meter, WIFI (optional), RF(optional), DRM, USB, ISO alarm, Parallel operation			
LCD display	Backlight 20*4 character				Backlight 20*4 character			
Standard warranty [years]	5-10				5-10			

*Can be modified without notice.(V2)

ANNEXURE A-11: MATLAB Code for Data Modelling

```
% This script assumes these variables are defined:
%
%   Input - input data.
%   Output - target data.

x = Input;
t = Output;

%Dimension and classification with PCA

coeff = transpose(pca(x));

% Choosing a Training Function

trainFcn = 'trainlm';  % Levenberg-Marquardt backpropagation.

% Creating a Fitting Network
hiddenLayerSize = 10;
net = fitnet(hiddenLayerSize,trainFcn);

% Setup Division of Data for Training, Validation, Testing
net.divideParam.trainRatio = 60/100;
net.divideParam.valRatio = 20/100;
net.divideParam.testRatio = 20/100;

% Train the Network
[net,tr] = train(net,coeff,t);

% Test the Network
y = net(coeff);
e = gsubtract(t,y);
performance = perform(net,t,y);
```

```
% View the Network
view(net)
% Plots
% Uncomment these lines to enable various plots.
%figure, plotperform(tr)
%figure, plottrainstate(tr)
%figure, ploterrhist(e)
%figure, plotregression(t,y)
%figure, plotfit(net,x,t)
```